Rev.Adv.Mater.Sci. 13 (2006) 125-161

# ELASTIC BEHAVIOR OF DEFECTS IN NANOMATERIALS I. MODELS FOR INFINITE AND SEMI-INFINITE MEDIA

**M. Yu. Gutkin**

Institute of Problems of Mechanical Engineering, Russian Academy of Sciences, Bolshoj 61, Vasil. Ostrov, St. Petersburg 199178, Russia

*Received: November 10, 2006*

**Abstract.** Elastic models for different defects (dislocations, disclinations, inclusions, and inhomogeneities) whose behavior forms the basis of plastic deformation and fracture in nanomaterials are reviewed. The solutions under discussion describe the elastic fields and energies of defects located in infinite homogeneous media, near flat free surfaces of half-spaces, or in vicinity of interphase boundaries in infinite bi-materials. In parallel with results of traditional description of elastic fields within the classical linear theory of elasticity, some basic solutions obtained within non-classical (strain gradient, nonlocal and gauge field) theories of elasticity are also discussed. It is demonstrated that the main achievement made in these non-classical approaches is the elimination of the classical singularities from the elastic fields at lines of dislocations and disclinations, as well as at edges of inclusions. A special attention is paid to the stress fields and nanoscopic elastic behavior of dislocations near interfaces described in the framework of strain gradient elasticity.

## 1. INTRODUCTION

Theoretical description and analytical modeling of mechanical behavior of nanomaterials are commonly based on the theory of defects. Generation and evolution of specific defect structures form the fundamentals of plastic deformation and fracture in solids. On the other hand, the development of defect arrangements is mainly controlled by the elastic fields of defects, their interaction with other defects and their ability to accommodate the elastic strains (caused by external loading or other factors), without speaking about temperature, strain rate, and other possible external parameters.

There are at least two general factors which make it difficult to adapt the traditional elastic models of defects to the case of nanomaterials. The first one is that the characteristic nanoscopic sizes of their components often occur to be of the same order of magnitude as the cores of defects (dislocations and disclinations), the regions where use of the classical linear theory of elasticity becomes incorrect. The second one is that the defect structures are generated and develop near interfaces (free surfaces, grain and interphase boundaries) whose density may be very high. Therefore, to correctly model the defect behavior in nanomaterials within a continuum approach, one has to address non-classical solutions for elastic fields of defects obtained with account for boundary conditions at least at the nearest interface. To date only first attempts of such kind have been made. The most of theoretical models of plastic deformation in nanomaterials are based on the traditional description of defects within the classical linear theory of elasticity and often neglect the solutions of appropriate boundary-value problems (e.g., see Ref. 1).

The main aim of the present paper is to provide a systematic overview of the existing solutions describing elastic fields and energies of defects (dislocations, disclinations, inclusions and inhomogeneities) located in infinite homogeneous media, near flat free surfaces of half-spaces, or in vicinity of interphase boundaries in infinite bi-materials. In parallel with results of traditional description of elastic fields within the classical linear theory of elasticity, we

Corresponding author: gutkin@def.ipme.ru

consider and discuss several solutions obtained within non-classical (strain gradient, nonlocal and gauge field) theories of elasticity.

## 2. DEFECTS IN HOMOGENEOUS INFINITE MEDIUM

It seems to be reasonable to start our discussion of elastic behavior of defects in nanomaterials with the case of a homogeneous infinite medium. First, the elastic fields and strain energies of defects, which have been obtained for this special case, may often be used as basic components of more complicated solutions of corresponding boundary-value problems, which describe the elastic properties of defects in heterogeneous or finite solids modeling nanomaterials. Second, these basic solutions are still widely used in development of first-approximation theoretical models of physical mechanisms of plastic deformation and fracture in nanocrystalline materials (see, e. g., Ref. 1). Although such an approach to theoretical modeling of the mechanical behavior of nanomaterials is not free of many lacks, it allows one to catch at least the main and characteristic features of the phenomena under study. Based on these reasons, let us briefly consider some well known and new solutions for stress fields and energies of defects (dislocations, disclinations and inclusions) in homogeneous infinite medium.

### 2.1. Dislocations in homogeneous infinite medium

General solutions for a curvilinear dislocation of arbitrary shape are given in many monographs on the theory of dislocations [2-7]. However, in practice of theoretical modeling, they commonly deal with some special cases of the shape of dislocation line. We restrict our attention to straight dislocations and closed dislocation loops.

#### 2.1.1. Straight dislocations in homogeneous infinite medium

Traditional description of elastic fields produced by dislocations is based on the classical theory of linear elasticity [2–9]. In the isotropic case, the appropriate expressions for elastic fields are quite simple and broadly applicable to model the structure and mechanical behavior of various materials and solid state systems.

Consider a mixed dislocation whose line coincides with the $z$-axis of a Cartesian coordinate system. Let its Burgers vector be $\mathbf{b} = b_x\mathbf{e}_x + b_z\mathbf{e}_z$ thus determining the edge ($b_x$) and screw ($b_z$) components. In the framework of classical elasticity theory, the total displacement field $\mathbf{u}^0$ is described by

$$\mathbf{u}^0 = \frac{b_x\mathbf{e}_x + b_z\mathbf{e}_z}{2\pi}\left\{\arctan\frac{y}{x} + \frac{\pi}{2}\,\mathrm{sgn}(y)\left[1 - \mathrm{sgn}(x)\right]\right\} + \frac{b_x}{4\pi(1-\nu)}\left\{\mathbf{e}_x\,\frac{xy}{r^2} - \mathbf{e}_y\left[(1-2\nu)\ln r + \frac{x^2}{r^2}\right]\right\}, \quad (1)$$

where $\nu$ is the Poisson ratio, $r^2 = x^2 + y^2$. Here we use a single-valued discontinuous form suggested by de Wit [10]. The elastic stress field $\sigma_{ij}^0$ is given (in units of $D = \mu/[2\pi(1-\nu)]$, where $\mu$ is the shear modulus) by [2-7,10]

$$\begin{aligned}
\sigma_{xx}^0 &= -b_x y\left(2x^2 + r^2\right)/r^4,\\
\sigma_{yy}^0 &= b_x y\left(2x^2 - r^2\right)/r^4,\\
\sigma_{xy}^0 &= b_x x\left(2x^2 - r^2\right)/r^4,\\
\sigma_{zz}^0 &= \nu\left(\sigma_{xx}^0 + \sigma_{yy}^0\right) = -b_x 2y/r^2,\\
\sigma_{xz}^0 &= -b_z(1-\nu)y/r^2,\\
\sigma_{yz}^0 &= b_z(1-\nu)x/r^2.
\end{aligned} \quad (2)$$

It is easy to see that the $y$-component of the displacement field (1) has the classical logarithmic singularity at the dislocation line ($r \to 0$), and the stress components (2) are also singular ($\sim r^{-1}$) there. These singularities are the principal lacks of the classical solutions that limit the applicability of the classical theory of elasticity to describe situations where it is important to know the strained state near dislocation lines.

The strain energy $W^0$ of the dislocation per unit dislocation length is [2-6]

$$W^0 = \frac{D}{2}\left[b_x^2 + (1-\nu)b_z^2\right]\ln\frac{R}{r_c}, \quad (3)$$

where $R$ denotes the size of the solid and $r_c$ is a cut-off radius for the dislocation elastic field near the dislocation line. When $r_c \to 0$, $W^0$ becomes singular.

Many attempts have been made to dispense with the classical singularities in elastic fields of dislocations and disclinations within a continuum theory (see, for a review, Refs. 11 and more recent publications [12-22]). We show below some results obtained within a simple gradient modification of the

classical linear theory of elasticity proposed by Ru and Aifantis in unpublished work [23]. The constitutive equation of this theory reads

$$\left(1-c_1\nabla^2\right)\boldsymbol{\sigma}=\left(1-c_2\nabla^2\right)\left[\lambda(\mathrm{tr}\,\boldsymbol{\varepsilon})\mathbf{I}+2\mu\boldsymbol{\varepsilon}\right] \tag{4}$$

where $\lambda$ and $\mu$ are the usual Lamé constants, $\boldsymbol{\sigma}$ and $\boldsymbol{\varepsilon}$ denote elastic stress and strain tensors, $\mathbf{I}$ is the unit tensor, $\nabla^2$ is the Laplacian, $c_1$ and $c_2$ are two different gradient coefficients. The authors [23] have proved that the solution of (4) may be obtained by using solutions of classical elasticity for the same traction boundary-value problem. In fact, the fields of displacements $\mathbf{u}$, strains $\boldsymbol{\varepsilon}$ and stresses $\boldsymbol{\sigma}$ are determined through the corresponding inhomogeneous Helmholtz equations

$$\begin{aligned}&\left(1-c_2\nabla^2\right)\mathbf{u}=\mathbf{u}^0,\ \left(1-c_2\nabla^2\right)\boldsymbol{\varepsilon}=\boldsymbol{\varepsilon}^0,\\&\left(1-c_1\nabla^2\right)\boldsymbol{\sigma}=\boldsymbol{\sigma}^0,\end{aligned} \tag{5}$$

with the classical solutions on the right hand sides, provided that appropriate care is taken for the extra (due to the higher order terms) boundary conditions or conditions at infinity. For dislocations and disclinations in a homogeneous medium, these solutions are accounted for by assuming that the strain and stress fields at infinity are the same for both the gradient and classical theory. Eqs. (5) can be solved [24-28] by using the Fourier transform method. For the total displacements, solution of $(5)_1$ gives [24,26,27,29]

$$\begin{aligned}\mathbf{u}=\mathbf{u}^0&-\frac{b_x}{4\pi(1-\nu)}\left\{\left[\mathbf{e}_x 2xy\right.\right.\\&\left.\left.+\mathbf{e}_y\left(y^2-x^2\right)\right]r^2\Phi_2+\mathbf{e}_y\Phi_0\right\}\\&+\frac{b_x\mathbf{e}_x+b_z\mathbf{e}_z}{2\pi}\,\mathrm{sgn}(y)\\&\times\int_0^{+\infty}\frac{s\sin(sx)}{1/c_2+s^2}\exp\left(-|y|\sqrt{\frac{1}{c_2}+s^2}\right)ds,\end{aligned} \tag{6}$$

where the classical solution $\mathbf{u}^0$ is given by (1),

$$\begin{aligned}\Phi_0&=(1-2\nu)K_0\left(r/\sqrt{c_2}\right),\\\Phi_2&=\frac{2c_2/r^2-K_2\left(r/\sqrt{c_2}\right)}{r^4}\end{aligned} \tag{7}$$

with $K_n(t)$ the modified Bessel function of the second kind and $n$ = 0,1,... the order of this function. Recently Lazar and Maugin [22] have noticed that formula (6) does not satisfy Eq. $(5)_1$ at the point ($y$ = 0) and obtained a corrected formula (see Eq. (2.36) in [22]).

For the stresses, the solution of $(5)_3$ gives [26,27] $\sigma_{ij}=\sigma_{ij}^0+\sigma_{ij}^{gr}$, where $\sigma_{ij}^0$ is given by (2) and $\sigma_{ij}^{gr}$ (in units of $2D$) by

$$\begin{aligned}\sigma_{xx}^{gr}&=b_x y\left[y^2\Phi_1+\left(3x^2-y^2\right)\Phi_2\right],\\\sigma_{yy}^{gr}&=b_x y\left[x^2\Phi_1-\left(3x^2-y^2\right)\Phi_2\right],\\\sigma_{xy}^{gr}&=-b_x x\left[y^2\Phi_1+\left(x^2-3y^2\right)\Phi_2\right],\\\sigma_{zz}^{gr}&=\nu\left(\sigma_{xx}^{gr}+\sigma_{yy}^{gr}\right)=b_x yr^2\Phi_1,\\\sigma_{xz}^{gr}&=b_z yr^2\Phi_1/2,\ \ \sigma_{yz}^{gr}=-b_z xr^2\Phi_1/2,\end{aligned} \tag{8}$$

with $\Phi_1=K_1\left(r\sqrt{c_1}\right)/\left(\sqrt{c_1}r^3\right)$. It is worth noting that the stress field (8) for screw dislocations (when $b_x$ = 0) are given by similar formulas in the nonlocal [30-32] and gauge field [12,14,16,33,34] theories. The solutions (8) for the screw and edge dislocations coincide with those in the gauge theory [14-16].

The main feature of the solutions given by (6)-(8) is the absence of any singularities in the displacement, strain and stress field. In fact, when $r\to 0$, we have $K_0\left(r/\sqrt{c_k}\right)\to-\gamma+\ln\left(2\sqrt{c_k}/r\right)$, where $\gamma$= 0.5772… is Euler's constant, $K_1\left(r/\sqrt{c_k}\right)\to\sqrt{c_k}/r$ and $K_2\left(r/\sqrt{c_k}\right)\to 2c_k/r^2-1/2$ ($k$ = 1,2). Hence, $u_y$ is finite as $\varepsilon_{ij}\to 0$ and $\sigma_{ij}\to 0$ at the dislocation line. The field of displacements (6) and strains have been analyzed in detail in [24,29] using a special version of the gradient elasticity theory ($c_1\equiv 0$). The stress fields (8) have been examined in [26]. They are also briefly reviewed in [1,11].

Using (8), one can find the strain energy of the dislocation within the gradient elasticity theory given by (4). The first calculation was carried out through the work done by the stress field (8) in producing the corresponding classical (for simplicity) plastic distortion [26]. The result (see also Refs. 1 and 11) was not singular at the dislocation line, in contract to (3), but contained only one gradient coefficient $c_1$, which looked strange. Later, a more general consideration operating with the classical formula $W=\frac{1}{2}\int_V\sigma_{ij}\varepsilon_{ij}dV$ has resulted in the formula [35]

$$W = \frac{D}{2}\left\{\frac{3b_x^2}{4(1-\nu)} + \left[b_x^2 + (1-\nu)b_z^2\right] \times\left(\gamma + \ln\frac{R}{2\sqrt{c_1}} + \frac{c_2}{2(c_1-c_2)}\ln\frac{c_2}{c_1}\right)\right\}, \quad (9)$$

which now contains both gradient coefficients $c_1$ and $c_2$.

In considering the straight dislocations in a homogeneous elastic isotropic solid within the gradient theory of elasticity described by (4), one can summarize [11] that gradient solution gives non-singular expressions for dislocation displacement, strain and stress fields and elastic energies. It has been shown that for individual dislocations, the elastic strains and stresses are strictly equal to zero at the dislocation lines and achieve their extreme values of ≈(3 ÷ 14)% and ≈(μ/4 ÷ μ/2), respectively, at a distance ≈$a_L$/4 ($a_L$ is the lattice parameter) from the dislocation line. Two characteristic distances appear naturally in this approach: $r_0 \approx 4\sqrt{c_2}$ which may be viewed as the radius of dislocation core and $d_0 \approx 10\sqrt{c_2}$ which may be viewed as the radius of strong short-range interaction between dislocations.

## 2.1.2. Dislocation loops in homogeneous infinite medium

Elastic fields and energies of planar dislocation loops in infinite homogeneous medium have been discussed by many authors [2-6,36-41,43-63]. Here we briefly consider some results for circular and rectangular loops which are often used in practice of 3D theoretical modeling.

Following [6], within classical isotropic linear elasticity, elastic fields of a circular glide dislocation loop were calculated by Koehler and used by Kröner [36], while those of a circular prismatic dislocation loop were obtained by Kroupa [37]. Marcinkowski and Sree Harsha [38] checked these results and corrected a number of errors in [36]. They also numerically analyzed in detail the stress distribution around a circular glide dislocation loop. Marcinkowski [39] studied the stress fields associated with coaxial arrays of such loops. The case of an elliptic dislocation loop with arbitrary Burgers vector was investigated by Mastrojannis *et al.* [40] who obtained the dislocation stresses, acting in the loop plane, in an explicit form.

The aforementioned solutions for elastic fields of circular dislocation loops were given through elliptic integrals. Later, Salamon and Dundurs [41] showed that these elastic fields may be given by compact forms involving the Lipschitz-Hankel integrals [42]. The corresponding solutions for prismatic [41,43,44] and glide [45] circular dislocation loops were first obtained for the case of two-phase elastically inhomogeneous solids with planar interfaces and after considered for a special case of identical elastic properties. Kolesnikova and Romanov [46-48] revisited these problems in the course of their systematic study of various circular dislocation-disclination loops for application to the method of virtual surface defects in different boundary-value problems in the theory of defects. They approved the results [41,43-45] and used circular prismatic dislocation loops as virtual defects for solving a number of boundary-value problems.

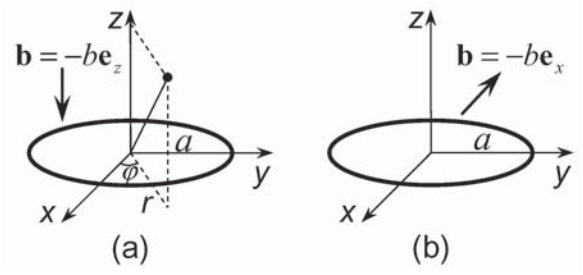


**Fig. 1.** Circular dislocation loops with Burgers vector **b** and radius *a* in an infinite homogeneous solid. (a) Intrinsic prismatic loop; (b) glide loop.

Following [41,43,44,46-48], for a circular interstitial prismatic dislocation loop shown in Fig. 1a, the total displacements read

$$u_r = \frac{b}{4(1-\nu)}\left[(2\nu-1)J(1,1;0) + \frac{|z|}{a}J(1,1;1)\right],$$
$$u_\varphi = 0,$$
$$u_r = \frac{b\,\mathrm{sgn}(z)}{4(1-\nu)}\left[2(1-\nu)J(1,1;0) + \frac{|z|}{a}J(1,0;1)\right], \quad (10)$$

where $b$ is the Burgers vector magnitude, $a$ the loop radius, $J(m,n;p)$ are Lipschitz-Hankel integrals given by [42] $J(m,n;p) = \int_0^\infty J_m(\kappa)J_n(\kappa r/a)\exp(-\kappa|z|/a)\cdot\kappa^p d\kappa$, and $J_m(\kappa)$ is the Bessel function of the first kind and $m$ the order of this function. The corresponding stress field is (in units of $\pi Db$)

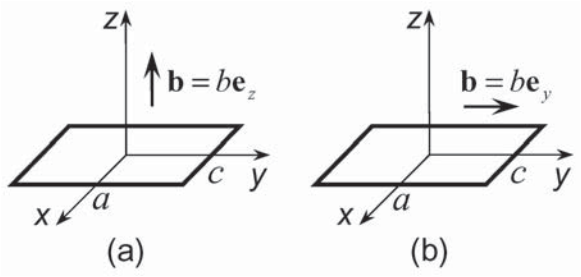


**Fig. 2.** Rectangular dislocation loops with Burgers vector **b** and sizes $2a \times 2c$ in an infinite homogeneous solid. (a) Prismatic loop; (b) glide loop.

$$
\begin{aligned}
\sigma_{rr} &= \frac{1-2\nu}{r} J(1,1;0) + \frac{|z|}{a^2} J(1,0;2) \\
&\quad - \frac{1}{a} J(1,0;1) - \frac{|z|}{ar} J(1,1;1), \\
\sigma_{\varphi\varphi} &= \frac{2\nu-1}{r} J(1,1;0) - \frac{2\nu}{a} J(1,0;1) + \frac{|z|}{ar} J(1,1;1), \\
\sigma_{zz} &= -\frac{1}{a} J(1,0;1) - \frac{|z|}{a^2} J(1,0;2), \\
\sigma_{rz} &= -\frac{z}{a^2} J(1,1;2), \\
\sigma_{z\varphi} &= \sigma_{r\varphi} = 0.
\end{aligned}
\tag{11}
$$

The strain energy of the circular prismatic dislocation loop was calculated as [43,46]

$$
W = \pi^2 Db^2 a J(1,1;0)\Big|_{r=a-r_c,\, z=0}. \tag{12}
$$

In the limiting case $a>>r_c$ formula (12) gives [46] $W \approx \pi Db^2$ a [ln($8a/r_c$)-2] which is rather close to the result given by formula (6-52) in [5].

According to [45-47], a circular glide dislocation loop (Fig. 1b) creates the total displacement field

$$
\begin{aligned}
u_r &= \frac{b\,\mathrm{sgn}(z)\cos\varphi}{4(1-\nu)} \left[ 2(1-\nu) J(1,0;0) - \frac{|z|}{a} J(1,0;1) \right. \\
&\quad \left. + \frac{|z|}{r} J(1,1;0) \right], \\
u_\varphi &= \frac{b\,\mathrm{sgn}(z)\sin\varphi}{4(1-\nu)} \left[ 2(\nu-1) J(1,0;0) \right. \\
&\quad \left. + \frac{|z|}{r} J(1,1;0) \right], \\
u_r &= \frac{b\cos\varphi}{4(1-\nu)} \left[ (1-2\nu) J(1,1;0) + \frac{|z|}{a} J(1,1;1) \right],
\end{aligned}
\tag{13}
$$

The stress field is (in units of $\pi Db$)

$$
\begin{aligned}
\sigma_{rr} &= \mathrm{sgn}(z)\cos\varphi \left[ -\frac{2}{a} J(1,1;1) \right. \\
&\quad \left. + \frac{|z|}{a^2} J(1,1;2) - \frac{|z|}{ar} J(1,2;1) \right], \\
\sigma_{\varphi\varphi} &= \mathrm{sgn}(z)\cos\varphi \left[ \frac{|z|}{ar} J(1,2;1) \right. \\
&\quad \left. - \frac{2\nu}{a} J(1,1;1) \right], \\
\sigma_{zz} &= -\cos\varphi \frac{|z|}{a^2} J(1,1;2), \\
\sigma_{z\varphi} &= \sin\varphi \left[ \frac{1-\nu}{a} J(1,0;1) \right. \\
&\quad \left. + \frac{\nu}{r} J(1,1;0) - \frac{|z|}{ar} J(1,1;1) \right], \\
\sigma_{rz} &= \cos\varphi \left[ -\frac{1}{a} J(1,0;1) + \frac{|z|}{a^2} J(1,0;2) \right. \\
&\quad \left. - \frac{|z|}{ar} J(1,1;1) + \frac{\nu}{r} J(1,1;0) \right], \\
\sigma_{r\varphi} &= \mathrm{sgn}(z)\sin\varphi \left[ -\frac{|z|}{ar} J(1,2;1) + \frac{1-\nu}{a} J(1,1;1) \right].
\end{aligned}
\tag{14}
$$

The strain energy of the circular glide dislocation loop is given by [45,46]

$$
W = \frac{\pi^2}{2} Db^2 a (2-\nu) J(1,1;0)\Big|_{r=a-r_c,\, z=0}. \tag{15}
$$

When $a>>r_c$ formula (15) results in [46] $W \approx \pi/2 Db^2 \times a(2-\nu)$[ln($8a/r_c$)-2]. The difference in square brackets is larger by ln2 than the corresponding difference in formula (6-51) in [5].

Circular dislocation loops are very convenient for modeling various physical (deformation, radiation, etc.) processes in the systems which possess axial or central symmetry. In more complicated situations, it is practical to use rectangular dislocation loops. For example, they may be utilized for construction of complex spatial dislocation configurations and models [49-54]. In recent years, the attention to rectangular dislocation loops increases [55,56] due to a possibility of their use in computer simulation of 3D dislocation dynamics.

Consider a rectangular extrinsic prismatic dislocation loop with Burgers vector $\mathbf{b} = b\mathbf{e}_z$ and sizes $2a \times 2c$ (Fig. 2a). The stress field of such a loop may be calculated by integrating the stress field of an infinitesimal dislocation loop over the surface of the loop under study [37]. The result reads (in units of $Db/2$) [57]

$$\sigma_{xx} = \frac{uv}{(u^2+z^2)\rho}\left[1-\frac{z^2}{\rho^2}-\frac{2z^2}{u^2+z^2}+2\nu\frac{u^2+z^2}{v^2+z^2}\right]\Bigg|_{x'=-a}^{x'=a}\Bigg|_{y'=-c}^{y'=c},$$

$$\sigma_{yy} = \frac{uv}{(v^2+z^2)\rho}\left[1-\frac{z^2}{\rho^2}-\frac{2z^2}{v^2+z^2}+2\nu\frac{v^2+z^2}{u^2+z^2}\right]\Bigg|_{x'=-a}^{x'=a}\Bigg|_{y'=-c}^{y'=c},$$

$$\sigma_{zz} = \frac{v}{u\rho}\left[\frac{z^2(4u^4+5u^2z^2+3z^4)}{u^2(u^2+z^2)^2}-\frac{z^4}{(u^2+z^2)\rho^2}\right.$$
$$\left.-\frac{2(u^2+v^2)}{v^2+z^2}+\frac{2z^2\rho^2}{(v^2+z^2)^2}+\frac{3(u^2-z^2)\rho^2}{u^2(v^2+z^2)}\right]\Bigg|_{x'=-a}^{x'=a}\Bigg|_{y'=-c}^{y'=c},$$

$$\sigma_{xy} = \frac{1}{\rho}\left[2\nu-\frac{u^2+v^2}{\rho^2}\right]\Bigg|_{x'=-a}^{x'=a}\Bigg|_{y'=-c}^{y'=c}, \qquad (16)$$

$$\sigma_{xz} = \frac{vz}{(u^2+z^2)\rho}\left[\frac{z^2}{\rho^2}-\frac{u^2-z^2}{u^2+z^2}\right]\Bigg|_{x'=-a}^{x'=a}\Bigg|_{y'=-c}^{y'=c},$$

$$\sigma_{yz} = \frac{uz}{(v^2+z^2)\rho}\left[\frac{z^2}{\rho^2}-\frac{v^2-z^2}{v^2+z^2}\right]\Bigg|_{x'=-a}^{x'=a}\Bigg|_{y'=-c}^{y'=c},$$

where $u = x - x'$, $v = y - y'$ and $\rho^2 = u^2 + v^2 + z^2$. As is seen, the stress components (16) are given by closed analytical forms in contrast with those of circular dislocation loops. This is one of the main reasons why the rectangular loops are very convenient for use in various applications.

The strain energy of the loop shown in Fig. 2a is (in units of $Db^2$) [58]

$$W = a\ln\frac{16a^2(\kappa-a)}{r_c^2(\kappa+a)}+c\ln\frac{16c^2(\kappa-c)}{r_c^2(\kappa+c)}-4(a+c-\kappa), \qquad (17)$$

where $\kappa^2 = a^2 + c^2$ and $(a,c) >> r_c/2$.

The stress field of a rectangular glide dislocation loop with Burgers vector $\mathbf{b} = b\mathbf{e}_y$ and sizes $2a \times 2c$ (Fig. 2b) may be calculated in a similar way that results (in units of $Db/2$) in [53]

$$\sigma_{xx} = \frac{uz}{(v^2+z^2)\rho}\left[1-2\nu-\frac{u^2}{\rho^2}\right]\Bigg|_{x'=-a}^{x'=a}\Bigg|_{y'=-c}^{y'=c},$$

$$\sigma_{yy} = \frac{uz}{(v^2+z^2)\rho}\left[-1-\frac{v^2}{\rho^2}-\frac{2v^2}{v^2+z^2}\right]\Bigg|_{x'=-a}^{x'=a}\Bigg|_{y'=-c}^{y'=c},$$

$$\sigma_{zz} = \frac{uz}{(v^2+z^2)\rho}\left[1-\frac{z^2}{\rho^2}-\frac{2z^2}{v^2+z^2}\right]\Bigg|_{x'=-a}^{x'=a}\Bigg|_{y'=-c}^{y'=c},$$

$$\sigma_{xy} = \frac{vz}{(u^2+z^2)\rho}\left[\nu-\frac{v^2}{\rho^2}\right]\Bigg|_{x'=-a}^{x'=a}\Bigg|_{y'=-c}^{y'=c}, \qquad (18)$$

$$\sigma_{xz} = \frac{1}{\rho}\left[-\nu+\frac{z^2}{\rho^2}\right]\Bigg|_{x'=-a}^{x'=a}\Bigg|_{y'=-c}^{y'=c},$$

$$\sigma_{yz} = \frac{uv}{(v^2+z^2)\rho}\left[1+(1-\nu)\frac{v^2+z^2}{u^2+z^2}-\frac{z^2}{\rho^2}-\frac{2z^2}{v^2+z^2}\right]\Bigg|_{x'=-a}^{x'=a}\Bigg|_{y'=-c}^{y'=c},$$

The strain energy of such a loop at $(a,c)>>r_c$ reads (in units of $Db^2$) [58]

$$W = a\ln\frac{16a^2(\kappa - a)}{r_c^2(\kappa + a)} + (1-\nu)c\ln\frac{16c^2(\kappa - c)}{r_c^2(\kappa + c)} - 2(2-\nu)(a + c - \kappa). \tag{19}$$

It is interesting to note that the strain energies of prismatic and glide dislocation loops become equal at $\nu \to 0$, in both the cases of circular and rectangular loops.Recently the stress field (18) and strain energy (19) have been used in development of 3D theoretical models [59-62] describing dislocation generation and deformation twinning in bulk nanocrystalline materials.

All the aforementioned solutions for dislocation loops were obtained within the classical linear theory of elasticity and therefore possess the same lacks as the solutions for straight dislocations; namely, the elastic fields and strain energies diverge in vicinity of dislocation lines. To dispense with this problem, Povstenko [63] used nonlocal theory of elasticity and obtained non-singular solutions for the stress fields of circular prismatic and glide dislocation loops. He also estimated their strain energies. However, the strain field singularities are still present in nonlocal elasticity.

## 2.2. Disclinations in homogeneous infinite medium

General geometric and elastic continual theory of disclinations is considered in serial reviews by de Wit [10,64,65] which are also collected in his book [66]. Geometry and elastic properties of disclinations as well as their behavior in different condensed media are discussed in detail in monographs [67-69]. As with dislocations, we briefly consider straight disclinations and closed disclination loops.

### 2.2.1. Straight disclinations in homogeneous infinite medium

In considering straight disclinations in an infinite medium, it is reasonable to start from the solutions for the so-called self-screened disclination configurations like two-axes dipoles [68,69], because the classical elastic fields for individual disclinations in infinite media contain the terms which are singular at infinity ($\sim r\ln r$ for displacements, $\sim\ln r$ for strains and stresses) and have no physical meaning (dimensional quantities under the logarithm signs). For brevity, however, we present below the general solution for an individual disclination obtained as a limiting case of a disclination dipole.

Consider a disclination of general type with Frank vector $\boldsymbol{\omega} = \omega_x\mathbf{e}_x + \omega_y\mathbf{e}_y + \omega_z\mathbf{e}_z$ in an infinite elastically isotropic medium. The scalars $\omega_x$ and $\omega_y$ determine the twist components of the disclination while $\omega_z$ determines its wedge component. Let its line coincides with the $z$-axis of the Cartesian coordinate system and the Frank vector is applied at the coordinate origin. For such an isolated disclination, the elastic fields themselves have no physical meaning because they are not screened but they may be used in modeling screened disclination configurations as basic elements [68,69].

Within the classical linear theory of elasticity, the stress field $\sigma_{ij}^0$ reads (in units of $D$) [10,66-69]

$$\begin{aligned}
\sigma_{xx}^0 &= \omega_x zx\left(y^2 - x^2\right)/r^4 - \omega_y zy\left(3x^2 + y^2\right)/r^4 + \omega_z\left(\ln r + y^2/r^2\right),\\
\sigma_{yy}^0 &= \omega_y zy\left(x^2 - y^2\right)/r^4 - \omega_x zx\left(x^2 + 3y^2\right)/r^4 + \omega_z\left(\ln r + x^2/r^2\right),\\
\sigma_{zz}^0 &= -2\nu\left[\omega_x zx/r^2 + \omega_y zy/r^2 - \omega_z\ln r\right],\\
\sigma_{xy}^0 &= \left(\omega_x y - \omega_y x\right)z\left(y^2 - x^2\right)/r^4 - \omega_z xy/r^2,\\
\sigma_{xz}^0 &= -\omega_x\left[(1-2\nu)\ln r + y^2/r^2\right] + \omega_y xy/r^2,\\
\sigma_{yz}^0 &= -\omega_y\left[(1-2\nu)\ln r + x^2/r^2\right] + \omega_x xy/r^2,
\end{aligned} \tag{20}$$

where $r^2 = x^2 + y^2$. As is seen, most of the components in (20) contain singular terms $\sim\ln r$.

In the framework of the gradient theory described by constitutive equation (4) and corresponding inhomogeneous Helmholtz equations (5), the solutions have been originally obtained for a disclination dipole

[11,27,28]. Solving $(5)_3$, we have finally for an individual disclination under consideration the stress field $\sigma_{ij} = \sigma_{ij}^0 + \sigma_{ij}^{gr}$, where $\sigma_{ij}^0$ are given by (20) and the gradient extra terms $\sigma_{ij}^{gr}$ (in units of $D$) by [11,27,28]

$$\begin{aligned}
\sigma_{xx}^{gr} &= \omega_x 2xz\left[y^2\Phi_1 + \left(x^2 - 3y^2\right)\Phi_2\right] \\
&\quad + \omega_y 2yz\left[y^2\Phi_1 + \left(3x^2 - y^2\right)\Phi_2\right] \\
&\quad + \omega_z\left[\Phi_0 + r^2\left(x^2 - y^2\right)\Phi_2\right], \\
\sigma_{yy}^{gr} &= \omega_x 2xz\left[x^2\Phi_1 - \left(x^2 - 3y^2\right)\Phi_2\right] \\
&\quad + \omega_y 2yz\left[x^2\Phi_1 - \left(3x^2 - y^2\right)\Phi_2\right] \\
&\quad + \omega_z\left[\Phi_0 - r^2\left(x^2 - y^2\right)\Phi_2\right], \\
\sigma_{zz}^{gr} &= 2\nu\left[\left(\omega_x x + \omega_y y\right)zr^2\Phi_1 + \omega_z\Phi_0\right] \\
\sigma_{xy}^{gr} &= \omega_x 2yz\left[-x^2\Phi_1 + \left(3x^2 - y^2\right)\Phi_2\right] \\
&\quad -\omega_y 2xz\left[y^2\Phi_1 + \left(x^2 - 3y^2\right)\Phi_2\right] + \omega_z 2xyr^2\Phi_2, \\
\sigma_{xz}^{gr} &= \omega_x\left[-\Phi_0 - r^2\left(x^2 - y^2\right)\Phi_2\right] - \omega_y 2xyr^2\Phi_2, \\
\sigma_{yz}^{gr} &= \omega_y\left[-\Phi_0 + r^2\left(x^2 - y^2\right)\Phi_2\right] - \omega_x 2xyr^2\Phi_2,
\end{aligned} \tag{21}$$

where $\Phi_i$ are the same as in Section 2.1.1. Using the limiting transitions noted in Section 2.1.1, it is easy to show the total elimination of classical logarithmic singularity from the superposition of elastic fields (20) and (21).

Examination of other characteristic features of the gradient solutions was given for elastic fields of two-axes disclination dipoles [11,27,28]. It was shown that within the gradient theory of elasticity described by (4), dipoles of straight disclinations of general type give zero or finite values for the elastic strains and stresses at the disclination lines. The finite values depend strongly on the dipole arm $d$ and show regular and monotonous (in the case of wedge disclinations) or nonmonotonous (in the case of twist disclinations) behavior for short-range (when $d<10\sqrt{c_k}$, $k$=1,2) interactions between disclinations. When the disclinations annihilate ($d\to 0$), the elastic strains and stresses tend regularly to zero values. Far from the disclination lines ($r>>10\sqrt{c_k}$), gradient and classical solutions coincide. When the dipole arm $d$ is much smaller than the scale unit $\sqrt{c_k}$, the elastic fields of a dipole of wedge disclinations transform into the elastic fields of an edge dislocation, as is the case in classical elasticity.

It is worth noting that similar results and conclusions for disclination elastic fields have recently been obtained by Lazar [17,18] within the field theory of elastoplasticity and by Lazar and Maugin [20] within the first strain gradient elasticity. Using nonlocal elasticity, Povstenko [70] also found nonsingular stress fields for straight disclinations, however the strain fields remained singular as always in this theory. Nonsingular solutions for elastic (strain, force stress, couple stress, double stress and bend-twist) fields of wedge disclinations were obtained by Lazar and Maugin [71] within gradient micropolar elasticity.

### 2.2.2. Disclination loops in homogeneous infinite medium

Comprehensive reviews of the literature on elastic fields and energies of planar disclination loops in infinite homogeneous medium are given in [67-69]. As with dislocation loops, the most of results were obtained for circular and rectangular disclination loops.

Within classical isotropic linear elasticity, elastic fields of circular disclination loops may be represented through the Lipschitz-Hankel integrals. Following [46,47], a pure circular wedge disclination loop characterized by Frank vector $\boldsymbol{\omega} = -\omega\mathbf{e}_y$ (Fig. 3a) creates the total displacement field

$$\begin{aligned}
u_r &= \frac{\omega a\cos\varphi}{8(1-\nu)}\left[(1-2\nu)J(2,0;0) + (2\nu-1)J(2,2;0)\right. \\
&\quad \left. -\frac{|z|}{a}J(2,0;1) + \frac{|z|}{a}J(2,2;1)\right], \\
u_\varphi &= \frac{\omega a\sin\varphi}{4(1-\nu)}\left[(2\nu-1)\frac{a}{r}J(2,1;-1) + \frac{|z|}{r}J(2,1;0)\right], \\
u_z &= \frac{\omega a\,\mathrm{sgn}(z)\cos\varphi}{4(1-\nu)}\left[2(1-\nu)J(2,1;0)\right. \\
&\quad \left. + \frac{|z|}{a}J(2,1;1)\right].
\end{aligned} \tag{22}$$

The corresponding stress field reads (in units of $\pi D\omega$) [46,47]

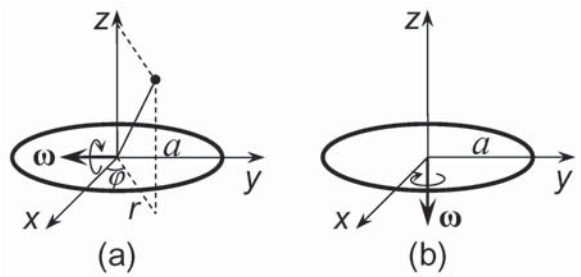


**Fig. 3.** Circular pure disclination loops with Frank's vector **ω** and radius *a* in an infinite homogeneous solid. (a) Wedge loop; (b) twist loop.

$$
\begin{aligned}
\sigma_{rr} &= \cos\varphi\left[(1-2\nu)\frac{a}{r}J(2,2;0) - J(2,1;1)\right.\\
&\quad \left. + \frac{|z|}{a}J(2,1;2) - \frac{|z|}{r}J(2,2;1)\right],\\
\sigma_{\varphi\varphi} &= \cos\varphi\left[(2\nu-1)\frac{a}{r}J(2,2;0) - 2\nu J(2,1;1)\right.\\
&\quad \left. + \frac{|z|}{r}J(2,2;1)\right],\\
\sigma_{zz} &= -\cos\varphi\left[J(2,1;1) + \frac{|z|}{a}J(2,1;2)\right],\\
\sigma_{z\varphi} &= \sin\varphi\,\frac{z}{r}J(2,1;1),\\
\sigma_{rz} &= \cos\varphi\left[\frac{z}{a}J(2,0;2) - \frac{z}{r}J(2,1;1)\right],\\
\sigma_{r\varphi} &= \sin\varphi\left[(1-2\nu)\frac{a}{r}J(2,2;0) - \frac{|z|}{r}J(2,2;1)\right].
\end{aligned}
\qquad (23)
$$

The strain energy of the pure circular wedge disclination loop is given by [46]

$$W = \frac{\pi^2}{2}D\omega^2 a^3 J(2,2;0)\Big|_{r=a-r_c,\ z=0}. \qquad (24)$$

When $a>>r_c$, formula (24) results in [46] $W \approx (\pi/2)D\omega^2 a^3[\ln(8a/r_c) - 8/3]$.

For a circular pure twist disclination loop with Frank vector $\boldsymbol{\omega} = -\omega\mathbf{e}_z$ (Fig. 3b), the field of total displacements has the only non-vanishing component $u_\varphi$ [46-48]:

$$u_\varphi = \frac{\omega a}{2}\,\mathrm{sgn}(z)J(2,1;0),\ \ u_r = u_z = 0. \qquad (25)$$

The stress field is (in units of $\pi(1-\nu)D\omega$) [46-48]

$$
\begin{aligned}
&\sigma_{r\varphi} = -\,\mathrm{sgn}(z)J(2,2;1),\ \ \sigma_{z\varphi} = -J(2,1;1),\\
&\sigma_{rr} = \sigma_{\varphi\varphi} = \sigma_{zz} = \sigma_{rz} = 0.
\end{aligned}
\qquad (26)
$$

The strain energy of the pure circular twis disclination loop reads [46]

$$W = \pi(1-\nu)D\omega^2 a^3 J(2,2;0)\Big|_{r=a-r_c,\ z=0}. \qquad (27)$$

At $a>>r_c$ formula (24) gives [46] $W \approx \pi(1-\nu)D\omega^2 a^3 \times[\ln(8a/r_c) - 8/3]$.

Circular twist disclination loops have been used as surface virtual defects for solution of a number of boundary-value problems. In particular, Kolesnikova and Romanov [46-48] utilized the elastic fields (25)-(26) to solve the problems for straight screw dislocations in a thin plate and a half-space when the dislocation line is normal to their free surfaces [46,47], circular twist disclination loops in a thin plate and a half-space when the loop plane is parallel to their free surfaces [46,47], and circular twist disclination loops parallel to a planar interface between two materials with different elastic moduli [46] or coaxial to a circular cylinder [48]. Sheinerman and Gutkin [72] took (25)-(26) to solve the problem of a cylindrical void (micropipe) containing a screw dislocation and perpendicular to the flat free surface of a half-space. Gutkin and Sheinerman [73] used formulas (26) to calculate the stress field of a radial step on the cylindrical surface of such a dislocated micropipe.

A common limitation of the abovementioned solutions is that the stress fields and energies are singular at the disclination line. Nonsingular solutions for stress fields of circular wedge and twist disclination loops were recently obtained by Povstenko and Matkovskii [74] within nonlocal theory of elasticity. However, as always in this theory, the strain fields remained singular.

Rectangular disclination loops in an infinite homogeneous medium were studied in detail by Pertsev *et al.* [75] who obtained the stresses and strain energies of twist and wedge disclination loops in terms of elementary functions, as is the case with rectangular dislocation loops (Section 2.1). These results are also reproduced in [68,69]. They were used in modeling the micromechanisms of plastic relaxation and disclination strengthening in polymers [76-78] and composite materials [76,79], see also [68,69] for more references.

## 2.3. Inclusions in homogeneous infinite medium

Nowadays both the micromechanics and physics of plastic deformation in heterogeneous and composite materials are based on such terms as *eigenstrain*, *eigenstress* and *inclusion*. By definition of Mura [80], "*Eigenstrain* is a generic name given by the author to such nonelastic strains as thermal expansion, phase transformation, initial strains, plastic strains, and misfit strains. *Eigenstress* is a generic name given to self-equilibrated internal stresses caused by one or several of these eigenstrains in bodies which are free from any other external force and surface constraint. The eigenstress fields are created by the incompatibility of the eigenstrains.<...>

When an eigenstrain $\varepsilon_{ij}^{*}$ is prescribed in a finite subdomain $\Omega$ in a homogeneous material $D$ (see Fig. 4) and it is zero in the matrix $D - \Omega$, then $\Omega$ is called an *inclusion*. The elastic moduli of the material are assumed to be homogeneous when inclusions are under consideration.

If a subdomain $\Omega$ in a material $D$ has elastic moduli different from those of the matrix, then $\Omega$ is called an *inhomogeneity*. Applied stresses will be disturbed by the existence of the inhomogeneity."

Goodier [81] was probably the first who studied elastic properties of inclusions. In his work, eigenstrains are the strains of thermal expansion. He considered both the ellipsoidal and rectangular inclusions embedded to a thin infinite plate. It was assumed that the plate temperature was zero everywhere except for the inclusion domains, where the temperature was nonzero and constant. Goodier's solution for the rectangular inclusion is also represented in textbooks [82,83] where one can find more references to early works on thermal stresses due to inclusions. In particular, Miklestad [84] investigated inclusions in the form of ellipsoid and homogeneously heated semi-infinite circular cylinder. Edward [85] solved the latter problem for an ellipsoidal inclusion having different elastic moduli, and studied stress concentration near spheroidal inclusions and cavities.

Attention to inclusion problems especially increased after publication of famous papers by Eshelby [86-88], collected also in a book [89]. They contain the solutions of problems on elastic fields of ellipsoidal inclusions subjected to arbitrary eigenstrain. Eshelby operated with imaginary procedures of cutting, distortion and gluing, and used Green's function in his calculations. He showed that

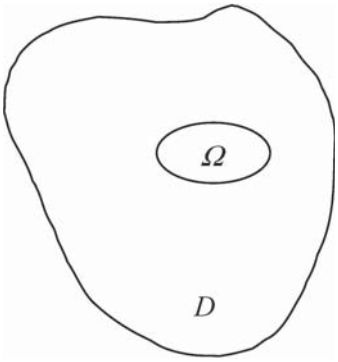


**Fig. 4.** Inclusion $\Omega$ in a homogeneous infinite material $D$.

in the case of a homogeneous eigenstrain, the elastic strains and stresses are constant inside the inclusion. The same is true when ellipsoidal inclusions are subjected to a system of homogeneous external forces applied at the infinity. The extension of this problem to the case of arbitrary anisotropies of matrix and inclusion was proposed in [80,90]. Kunin and Sosnina [90] considered a more general case of inhomogeneous external forces. Anisotropic inclusions were also studied in [91-98] for different kinds of elastic anisotropy and inclusion shape. A further extension to the case of a homogeneous inclusion, which possesses rheological properties of any complexity (nonlinear elastic, elasto-plastic or even visco-elasto-plastic) and is embedded in a linear elastic medium, was done by Vakulenko and Sevostianov [99-101]. A review of inclusion problems with inelastic matrix may be found in [102]. It is worth also to note the problems on inclusions which are separated from matrix by sliding interfaces [103-110].

The brief and clear presentation of Eshelby's results with many special cases and applications is contained in [80,111], where some further solutions of inclusion problems and their application to calculation of overall macroscopic properties of heterogeneous materials are considered. Relatively recent works of the end of the XX century are briefly analyzed in [102,112]. Among the most recent publications, we note the paper by Bert *et al.* [113] who give a detailed description of elastic fields and energy of an elastically isotropic spherical inclusion with one-dimensional dilatation eigenstrain.

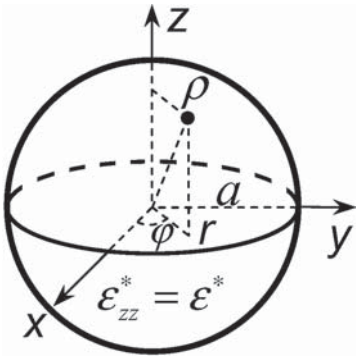


**Fig. 5.** Spherical inclusion with 1D dilatation eigenstrain ε* in an infinite homogeneous solid.

Following Bert *et al.* [113], if a spherical inclusion possesses a one-dimensional dilatation eigenstrain in the form $\varepsilon^*_{zz} = \varepsilon^*$, then in the cylindrical coordinate system (r,φ,z) with the origin at the inclision center (Fig. 5), the total displacement field $u_i^{(out)}$ outside the inclusion reads (in units of $\varepsilon^* R_{sp}/[30(1-\nu)]$, where $R_{sp}$ is the inclusion radius)

$$
\begin{aligned}
u_r^{(out)} &= \frac{\tilde r}{\tilde\rho^7}\Big[3\tilde r^2 - 5(1-2\nu)\tilde r^4 \\
&\quad +5(1+4\nu)\tilde r^2\tilde z^2 - 12\tilde z^2 + 10(1+\nu)\tilde z^4\Big], \\
u_\varphi^{(out)} &= 0, \\
u_z^{(out)} &= \frac{\tilde z}{\tilde\rho^7}\Big[9\tilde r^2 + 5(1-2\nu)\tilde r^4 \\
&\quad + 5(5-4\nu)\tilde r^2\tilde z^2 - 6\tilde z^2 + 10(2-\nu)\tilde z^4\Big],
\end{aligned}
\tag{28}
$$

where $\tilde r = r/R_{sp}$, $\tilde z = z/R_{sp}$, $\tilde\rho = \rho/R_{sp}$, and $\rho^2 = r^2 + z^2$. Inside the inclusion, the total displacement field $u_i^{(in)}$ is (in the same units)

$$
\begin{aligned}
u_r^{(in)} &= 2(5\nu-1)\tilde r, \\
u_\varphi^{(in)} &= 0, \\
u_z^{(in)} &= 2(7-5\nu)\tilde z.
\end{aligned}
\tag{29}
$$

The corresponding stress field $\sigma_{ij}^{(out)}$ outside the inclusion is given by (in units of $\mu\varepsilon^*/[15(1-\nu)]$)

$$
\begin{aligned}
\sigma_{rr}^{(out)} &= \frac{1}{\tilde\rho^9}\Big[-12\tilde r^4 + 10(1-\nu)\tilde r^6 + 81\tilde r^2\tilde z^2 \\
&\quad -15(3+2\nu)(\tilde r^2+\tilde z^2)\tilde r^2\tilde z^2 - 12\tilde z^4 + 10(1-\nu)\tilde z^6\Big], \\
\sigma_{\varphi\varphi}^{(out)} &= \frac{1}{\tilde\rho^7}\Big[3\tilde r^2 - 5(1-4\nu)\tilde r^4 + 5\tilde r^2\tilde z^2 \\
&\quad +10\nu\tilde r^2\tilde z^2 - 12\tilde z^2 + 10(1-\nu)\tilde z^4\Big], \\
\sigma_{zz}^{(out)} &= \frac{1}{\tilde\rho^9}\Big[9\tilde r^4 + 5\tilde r^6 - 72\tilde r^2\tilde z^2 + 45\tilde r^4\tilde z^2 \\
&\quad + 24\tilde z^4 - 40\tilde z^6\Big], \\
\sigma_{rz}^{(out)} &= \frac{3\tilde r\tilde z}{\tilde\rho^9}\Big[-3\tilde r^2 + \tilde r^4 - 3\tilde r^2\tilde z^2 + 4\tilde z^2 - 4\tilde z^4\Big], \\
\sigma_{r\varphi}^{(out)} &= \sigma_{z\varphi}^{(out)} = 0.
\end{aligned}
\tag{30}
$$

Inside the inclusion, the stress field $\sigma_{ij}^{(in)}$ is (in the same units)

$$
\begin{aligned}
&\sigma_{rr}^{(in)} = \sigma_{\varphi\varphi}^{(in)} = -2(5\nu+1), \quad \sigma_{zz}^{(in)} = -16, \\
&\sigma_{rz}^{(in)} = \sigma_{r\varphi}^{(in)} = \sigma_{z\varphi}^{(in)} = 0.
\end{aligned}
\tag{31}
$$

The strain energy of such an inclusion reads [113]

$$
W^{I} = \frac{32\pi\mu\left(\varepsilon^*\right)^2}{45(1-\nu)}R_{sp}^3,
\tag{32}
$$

where the upper index I means that the dilatation eigenstrain is one-dimensional (1D). As follows from Eshelby's theory [86,89], the strain energy of an inclusion of arbitrary shape, which possesses a 3D homogeneous dilatation $3\varepsilon^*$, is given by $W^{III} = 2\mu(1+\nu)/(1-\nu)(\varepsilon^*)^2 V$, where $V$ is the inclusion volume. For a spherical inclusion of radius $R_{sp}$ this formula gives $W^{III} = 2\pi\mu(1+\nu)/[3(1-\nu)](\varepsilon^*)^2 R_{sp}^3 \approx 5W^{I}$ at $\nu = 0.3$.

Bert *et al.* [113] used the energies (12), (32) and stress field (30), rewritten in the spherical coordinate system with the origin in the inclusion center, to study plastic relaxation near As-Sb nanoclusters in GaAs by generation of circular prismatic dislocation loops.

Let us consider now the cuboidal inclusions. For the 2D problem of a rectangular inclusion in a thin infinite plate, Goodier [81] (see also [82,83]) showed that thermoelastic strains and stresses are not homogeneous inside the inclusion as was the case

with an ellipsoidal inclusion. Besides, the shear strains and stresses occurred singular at the corners of the rectangular. The extension of this solution to the 3D case of a heated domain in the form of a parallelepiped was done by Ignaczak and Nowacki in 1958 and published in [114]. Lavrenyuk [115] studied the thermoelastically strained state of an infinite medium with a finite number of cuboidal inclusions whose faces were parallel to the coordinate planes. These results as well as many other solutions to the problems of thermoelastic inclusions are represented in [116].

Sass *et al.* [117] were probably the first who considered the elastic fields of a 3D cuboidal inclusion with a general homogeneous eigenstrain. For the case of elastic isotropy, they found the displacement field in terms of Fourier series. Using Eshelby's method, Faivre [118] calculated the elastic strain field of an isotropic cuboidal inclusion. He showed that if the eigenstrain is a pure dilatation $\varepsilon^*$, then the elastic dilatation is homogeneous and equal to $\varepsilon^*(1 + \nu)/[3(1 - \nu)]$ inside the inclusion and zero outside it. This means that the strain energy density of such an inclusion does not depend on its shape in total accordance with Eshelby's conclusion. Sankaran and Laird [119] used the solution of Kelvin's problem of a concentrated force to find the elastic strains of an elastically isotropic inclusion in the form of a square plate. Isotropic solution for a cuboidal inclusion was also obtained by Chiu [120].

The effect of elastic anisotropy on the elastic fields of cuboidal inclusions was investigated by Lee and Johnson [121] who showed for the exemplary case of copper that the account for anisotropy weakly influences the distribution of elastic strains either inside or outside the inclusion. However, there was a qualitatively new effect that for a homogeneous and purely dilatation eigenstrain of the inclusion, the elastic dilatation is inhomogeneous inside it (increasing from its center to periphery) and nonzero in the matrix. The strain energy of such an inclusion occurs to be smaller by 7% than that of a similar spherical inclusion of the same volume. It is worth noting that in the isotropic case, Faivre [118] obtained an opposite relation between these energies.

Some of the aforementioned models are discussed in the review by Li [122] with application to the problems of physical chemistry and materials science. The elastic models of inclusions in an infinite solid are often used to explain and predict the morphology of precipitates in crystalline [123-128] and amorphous [129] metals and alloys, and to develop physical models of residual stress relaxation in heterogeneous materials [51,130-141] and nanostructures [113,142].

The most of inclusion problems have been solved either by means of classical methods of the theories of elasticity and thermoelasticity or using various modifications of Eshelby's method combined with Green's function technique. However, since early 70-ies of the XX century, an alternative approach has been applied to these problems. This approach is based on wide use of the dislocation theory. Eshelby [86,89] noted that his method may be interpreted as continuous distribution of dislocations or dislocation loops over the inclusion boundary. The sum elastic fields of this continuous dislocation arrangement gives the solution of the inclusion problem. One can find the same idea in the paper by Faivre [118]. In a general form, this approach (called the method of virtual surface dislocations) was formulated by Kroupa and Lejček [143] who gave general solutions for the elastic fields of an isotropic 3D inclusion of arbitrary shape and a cylindrical inclusion of arbitrary cross-section. As an example, they analyzed the elastic model of a twin in the form of a cylinder with rectangular cross-section, strained by homogeneous shear and embedded into an infinite medium with the same elastic properties.

Later the method of virtual surface dislocations was used to calculate the stress fields of lamellar terminations (typical imperfections in the lamellar structure of unidirectionally-solidified eutectic composites) [51,57], rod-like defects in silicon crystals [52], steps at interphase boundaries [140], foreign polytype inclusion in silicon carbide [141], and coherent embryos of ferrite in austenitic matrix [144,145]. Below we consider this method in more details taking an elastically isotropic cuboidal inclusion as an example.

Let the cuboidal inclusion have the sizes $2a \times 2b \times 2c$ and be located in an elastically isotropic infinite medium having the same elastic moduli as the inclusion. It is supposed that the inclusion is characterized by a 3D purely dilatation eigenstrain $\varepsilon^*$ due to misfit in the lattice parameters $a_1$ and $a_2$, and difference in the coefficients of thermal expansion $\alpha_1$ and $\alpha_2$ of the inclusion and matrix, respectively. The lattice misfit is described by ratio $f = 2(a_1 - a_2)/a_2$, while the thermal expansion misfit by parameter $g = (\alpha_1 - \alpha_2)\Delta T$, where $\Delta T = T_{cr} - T$, $T_{cr}$ is the temperature of crystallization for the system matrix-inclusion and $T$ is the current temperature. The eigenstrain is then given by $\varepsilon^* = f - g$.

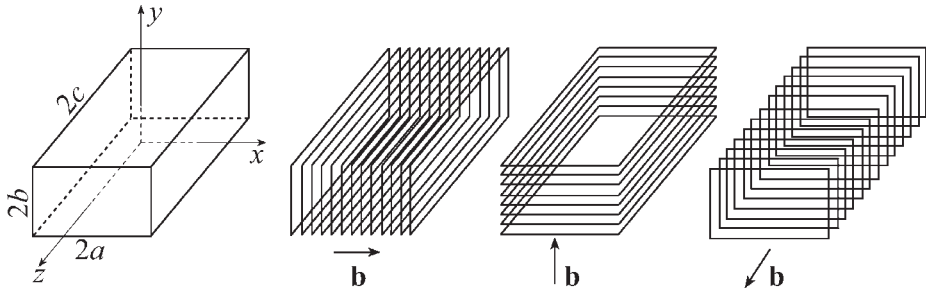


**Fig. 6.** Cuboidal inclusion and its dislocation model consisting of three rows of continuously distributed rectangular prismatic dislocation loops.

Following [86,89,122,143], the arrangement of virtual dislocations, modeling the elastic fields of the inclusion, may be composed of three rows of rectangular prismatic dislocation loops continuously distributed over the inclusion faces (Fig. 6). The product of their Burgers vector magnitude $b$ and distribution density $\eta$ gives the eigenstrain value: $\varepsilon^* = b\eta$. The elastic fields of the inclusion are calculated by integration of the corresponding elastic fields of a virtual dislocation loop over its row, and by the sum of the integration results for each of the three rows. For example, the stress field of a virtual loop is given by formulas (16). After integration and summation, the final result reads [140,144,145]

$$\sigma_{ij}(x,y,z) = C\Psi_{ij}(x-x', y-y', z-z')\Big|_{x'=x_1}^{x'=x_2}\Big|_{y'=y_1}^{y'=y_2}\Big|_{z'=z_1}^{z'=z_2}, \tag{33}$$

where $C = D\varepsilon^*(1+\nu)$,

$$\Psi_{xx} = \arctan\frac{u\rho}{vt}, \quad \Psi_{yy} = \arctan\frac{v\rho}{ut},$$
$$\Psi_{zz} = \arctan\frac{t\rho}{uv}, \quad \Psi_{xy} = -\ln(\rho+t), \tag{34}$$
$$\Psi_{xz} = -\ln(\rho+v), \quad \Psi_{yz} = -\ln(\rho+u),$$

$u = x - x'$, $v = y - y'$, $t = z - z'$, $\rho^2 = u^2 + v^2 + t^2$, and $x_k$, $y_k$, $z_k$ ($k$ = 1,2) are the coordinates of the inclusion corners. For the inclusion in Fig. 6, we have $x_1 = -a$, $x_2 = a$, $y_1 = -b$, $y_2 = b$, $z_1 = -c$, and $z_2 = c$.

The strain energy of the inclusion is given by $W = 16\mu(1+\nu)/(1-\nu)(\varepsilon^*)^2abc$.

It is seen that the shear components of the stress tensor $\sigma_{ij}$ ($i \neq j$) logarithmically diverge at the inclusion corners as well as at the edges normal to the plane ($ij$). The normal components $\sigma_{ij}$ ($i = j$) do not diverge but suffer the jumps at the faces with normals $n_k$ if ($i \neq k$). The hydrostatic component $\sigma = \mathrm{tr}\sigma_{ij}/3$ is constant and equal to $-8\pi C/3$ inside the inclusion and zero outside it. All of these characteristic features of the inclusion stress field appear within the approach of the classical isotropic linear theory of elasticity. One could expect that they will disappear in the framework of a generalized (nonlocal, or nonlinear, or gradient, etc.) theory of elasticity. Here we can demonstrate this in the exemplary case of a long rod-like inclusion with a rectangular cross section [146].

Let $c \to \infty$ in stress components (33)-(34) which then transform into the following classical solution

$$\sigma_{ij}^0(x,y) = 2C\Psi_{ij}^0(x-x', y-y')\Big|_{x'=x_1}^{x'=x_2}\Big|_{y'=y_1}^{y'=y_2}, \tag{35}$$

with

$$\Psi_{xx}^0 = -\arctan\frac{u}{v}, \quad \Psi_{yy}^0 = -\arctan\frac{v}{u},$$
$$\Psi_{zz}^0 = \Psi_{xx}^0 + \Psi_{yy}^0 = -\frac{\pi}{2}\mathrm{sgn}\frac{u}{v}, \tag{36}$$
$$\Psi_{xy}^0 = \ln r, \quad \Psi_{xz}^0 = \Psi_{yx}^0 = 0,$$

where $r^2 = u^2 + v^2$.

Within the strain gradient theory of elasticity described by equations (4) and (5), the stress field is written as $\sigma_{ij} = \sigma_{ij}^0 + \sigma_{ij}^{(gr)}$, where the classical terms are given by (35) and (36), while the gradient extra terms are (in units of $2C$ ) [146]

$$\sigma_{xx}^{(gr)} = -2\,\mathrm{sgn}(v) \times \int_0^{+\infty} \frac{\sin(sa)\cos(sx)}{s} e^{-\lambda|v|} ds \Bigg|_{y'=-b}^{y'=b},$$
$$\sigma_{yy}^{(gr)} = -2\,\mathrm{sgn}(u) \times \int_0^{+\infty} \frac{\sin(sb)\cos(sy)}{s} e^{-\lambda|u|} ds \Bigg|_{x'=-a}^{x'=a},$$
$$\sigma_{zz}^{(gr)} = \sigma_{xx}^{(gr)} + \sigma_{yy}^{(gr)}, \quad (37)$$
$$\sigma_{xy}^{(gr)} = K_0\left(r/\sqrt{c_1}\right)\Big|_{x'=-a}^{x'=a}\Big|_{y'=-b}^{y'=b},$$
$$\sigma_{xz}^{(gr)} = \sigma_{yz}^{(gr)} = 0,$$

where $\lambda = \sqrt{s^2 + 1/c_1}$. Let us consider in more details the component $\sigma_{xy}$ which is singular at the inclusion edges within the classical elasticity. The gradient solution for this component is given by the sum

$$\sigma_{xy}(x,y) = 2C\left[\ln r + K_0\left(r/\sqrt{c_1}\right)\right]\Big|_{x'=-a}^{x'=a}\Big|_{y'=-b}^{y'=b}. \quad (38)$$

Using the asymptotics $K_0\left(r/\sqrt{c_1}\right)\big|_{r\to 0} \approx -\gamma - \ln\left(r/\sqrt{c_1}\right)$, where $\gamma = 0.5772...$ is Euler's constant, one can calculate the shear stress values just at the inclusion edges. For example, at the edge ($x = a$, $y = b$) it is

$$\sigma_{xy}(a,b) \approx -2C\left[\ln\frac{ab}{\sqrt{c_1\left(a^2+b^2\right)}} + \gamma + K_0\left(\frac{2a}{\sqrt{c_1}}\right) + K_0\left(\frac{2b}{\sqrt{c_1}}\right) - K_0\left(\frac{2\sqrt{a^2+b^2}}{\sqrt{c_1}}\right)\right]. \quad (39)$$

This formula demonstrates a size effect when the shear stress at the inclusion corners depends on the inclusion sizes. For the square cross section $2a\times 2a$, we obtain very simple asymptotic formulas for the limiting cases $a >> \sqrt{c_1}$ and $a \to 0$:

$$\sigma_{xy}(a)\Big|_{a>>\sqrt{c_1}} \approx -\gamma - \ln\frac{a}{\sqrt{2c_1}}, \quad \sigma_{xy}(a)\Big|_{a\to 0} \to 0. \quad (40)$$

In fact, the first of these asymptotics is valid even for nanoscopic inclusions (like quantum dots or nanowires) because the gradient coefficients in (4) and (5) are commonly estimated [11,26,147] as $\sqrt{c_1} \approx \sqrt{c_2} \approx a_L/4$, where $a_L$ is the lattice parameter. One can conclude that the magnitude of shear stress at the inclusion edges grows logarithmically with its size.

For comparison, the classical and gradient solutions for stress components $\sigma_{xx}$, $\sigma_{xy}$ and $\sigma$ are represented by 3D plots in Fig. 7. They show that the gradient solution is free from the stress jumps at the inclusion faces (Figs. 7a and 7c) and stress singularities at its corners (Fig. 7b). Besides, the hydrostatic stress component $\sigma$ is not constant inside the inclusion and zero outside it, but is described by a smooth function of coordinates (Fig. 7c). This seems to be important for modeling diffusion in stress fields of inclusions as is the case with edge dislocations [148].

In recent years, similar conclusions have been made within various nonlocal and strain gradient theories mainly addressed normal strains and dilatation of quantum dots and nanowires of different shapes (e.g., see [149-151]) due to their importance for nano-optics and nanoelectronics.

## 3. DEFECTS NEAR PLANAR INTERFACES IN INFINITE AND SEMI-INFINITE MEDIA

A description of the elastic behavior of defects near planar interfaces (free surfaces, grain and phase boundaries) has been one of the key problems in the theory of defects, with applications to materials science and engineering and special attention to polycrystalline, multilayered and thin-film solid systems (e.g., see [5,152-160]). This description is traditionally based on solutions of appropriate boundary-value problems in the classical linear theory of elasticity. The corresponding solutions provide the elastic fields of defects far from both the interface and the defect itself, thus being satisfactory for the cases when long-range elastic interactions are of interest. However, when short-range interactions are of interest, the classical solutions lead to unreasonable results. For example, in the case of dislocations, this concerns the elastic singularity at the dislocation line, as well as the 'image' force which acts on dislocations from the side of an interface which also becomes singular when the dislocation approaches the interface. Moreover, some components of the elastic stress field of a dislocation suffer jumps at the interface, a fact which may be acceptable from a macroscopic point of view but physi-

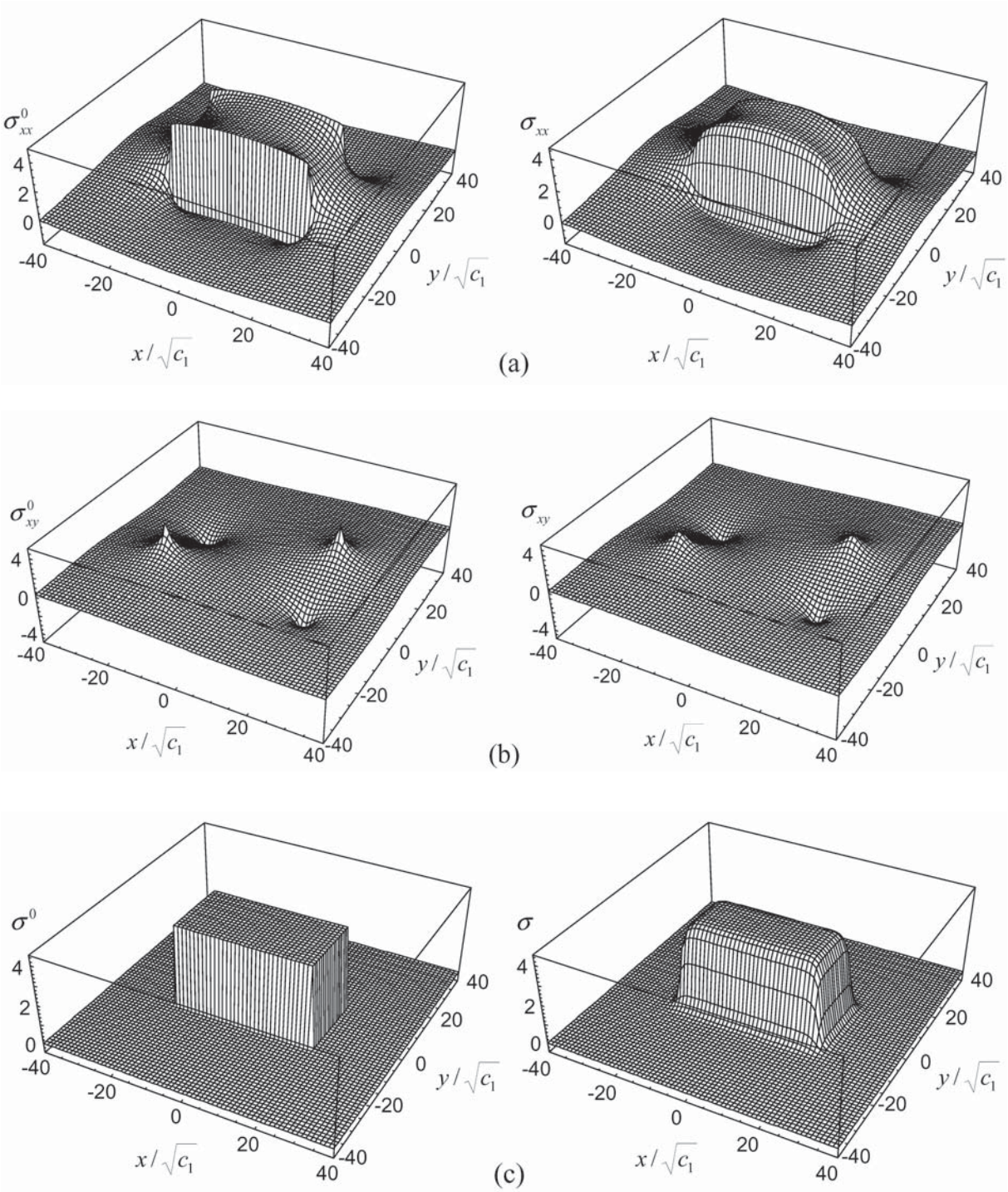


**Fig. 7.** Classical (left) and gradient (right) solutions for the stress components of a rod-like inclusion with the rectangular cross section and sizes $2a = 20\sqrt{c_1}$ and $2b = 10\sqrt{c_1}$. (a) The *xx*-component, (b) the *xy*-component, (c) the hydrostatic component. The stress values are given in units of $2C = \mu\varepsilon^*(1 + \nu)/[\pi(1 - \nu)]$.

cally unrealistic from a nano- or microscopic point of view. Therefore, in parallel with classical solutions, we briefly consider some gradient solutions obtained recently for dislocations [11,161-163], which allow one to dispense with difficulties of classical theory.

## 3.1. Dislocations near planar interfaces

As before (in Section 2.1), we separately consider the most practical cases of straight dislocations and closed dislocation loops.

### 3.1.1. Straight dislocations parallel to flat interfaces

Consider a flat interface which separates two elastic isotropic media denoted by 1 ($x > 0$) and 2 ($x < 0$) with shear moduli $\mu_i$ and Poisson ratios $\nu_i$, where $i = 1,2$, respectively. Let a straight dislocation having Burgers vector $\mathbf{b} = b_x\mathbf{e}_x + b_y\mathbf{e}_y + b_z\mathbf{e}_z$ goes through the point ($x = x'$, $y = 0$) along the $z$-axis of a Carthesian coordinate system.

Within the classical linear isotropic theory of elasticity, Head [164,165] was the first who solved this problem for the cases of screw (when $b_x = b_y \equiv 0$) [164] and edge (when $b_z \equiv 0$) [165] dislocations. These solutions are also represented in many reviews and monographs (e.g., see [11,152-154] and [5,80], respectively) devoted to dislocation theory. Here we use the form suggested in [152].

#### 3.1.1.1. Screw dislocation

The classical solution for a *screw* dislocation shown in Fig. 8 is given in medium 1 by [in units of $\mu_1 b_z/(2\pi)$]

$$\sigma_{xz}^{0(1)} = -\frac{y}{r_-^2} + \frac{\Gamma-1}{\Gamma+1}\frac{y}{r_+^2},$$
$$\sigma_{yz}^{0(1)} = \frac{x-x'}{r_-^2} + \frac{\Gamma-1}{\Gamma+1}\frac{x+x'}{r_+^2}, \qquad (41)$$

and in medium 2 by

$$\sigma_{xz}^{0(2)} = -\frac{2\Gamma}{\Gamma+1}\frac{y}{r_-^2}, \quad \sigma_{yz}^{0(2)} = \frac{2\Gamma}{\Gamma+1}\frac{x-x'}{r_-^2}, \qquad (42)$$

where $r_\pm^2 = (x \pm x')^2 + y^2$ and $\Gamma = \mu_2/\mu_1$. The upper index 0 shows that stress components (41) and (42) were obtained within the classical theory of elasticity.

It is easily seen that the component $\sigma_{xz}^0$ is continuous at the interface ($x = 0$) while the component $\sigma_{yz}^0$ suffers a jump there, given by the expression

$$\left[\sigma_{yz}^0\right]_{x=0} = \sigma_{yz}^{0(1)}(x=0) - \sigma_{yz}^{0(2)}(x=0)$$
$$= \frac{\mu_1 b_z}{\pi}\frac{\Gamma-1}{\Gamma+1}\frac{x'}{x'^2+y^2}. \qquad (43)$$

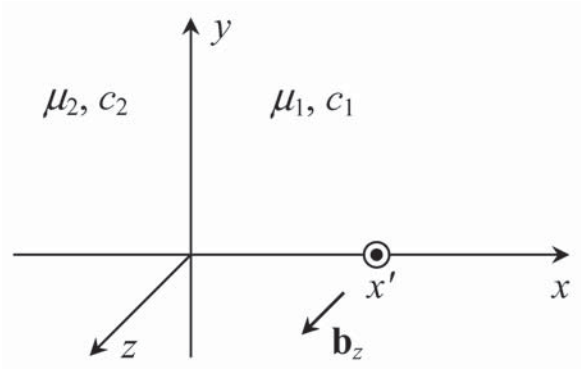


**Fig. 8.** Screw dislocation near a flat interface between the materials having different shear moduli $\mu_1$ and $\mu_2$, and different gradient coefficients $c_1$ and $c_2$.

Such jump is expected from the macroscopic viewpoint of classical elasticity because this $yz$-component does not give any contribution to the $x$-component of the elastic force which has to be in equilibrium at the interface. On the other hand, in considering the stressed state of an ideally welded interface from a nanoscopic point of view, the nature of this jump is not quite clear. In fact, the atomic layers on both sides of the interface interact elastically not only with atoms of their own material but also with atoms of the opposite material. Therefore, one has to assume the existence of a transitional zone of a few atomic layers where elastic interactions between atoms vary smoothly from stronger ones which are characteristic of one bulk material, to weaker ones which are characteristic of the other bulk material. It follows from this assumption, that a stress jump like (43) is only a consequence of the approximation of classical continuum models which often become insufficient for describing nanoscale phenomena.

To demonstrate this fact, we note that the stress jump in (43) tends to infinity in the plane ($xz$) when the dislocation approaches the interface. It may thus be desirable for the interface stress jump to be eliminated from the solution of this problem within any generalized theory of elasticity aiming to consider nanoscale phenomena.

Let us now discuss the corresponding dislocation fields within the theory of gradient elasticity given by (4). As proposed in [23] and described also in [26,28], one can obtain the solution of (4) by considering separately Eqs. $(5)_2$ and $(5)_3$ in terms of the

strain $\boldsymbol{\varepsilon}^0$ and stress $\boldsymbol{\sigma}^0$ fields of the classical elasticity theory for the same boundary-value problem. Following [161,162], here we consider only the solution of Eq. $(5)_3$ for the stress field since it is especially important for applications.

Eq. $(5)_3$ can be solved [24-28] by using the Fourier transform method. First we rewrite it in the form

$$\left(1-c_{1i}\nabla^2\right)\boldsymbol{\sigma}^{(i)}=\boldsymbol{\sigma}^{0(i)}, \tag{44}$$

where $\boldsymbol{\sigma}^{0(i)}$ are given by (41) and (42). Below we omit for simplicity the first index '1' in the gradient coefficients $c_{1i}$; thus $c_1$ refers to material 1 and $C_2$ to material 2. Based on the above discussion of the stress jump at the interface, as well as on conclusions of Ru and Aifantis [23,166], we use the classical boundary condition

$$\left[\sigma_{xz}\right]_{x=0}=\sigma_{xz}^{(1)}(x=0)-\sigma_{xz}^{(2)}(x=0)=0 \tag{45}$$

and three extra boundary conditions

$$\begin{aligned}&\left[\sigma_{yz}\right]_{x=0}=\sigma_{yz}^{(1)}(x=0)-\sigma_{yz}^{(2)}(x=0)=0,\\&\left[\frac{\partial\sigma_{jz}}{\partial x}\right]_{x=0}=\left.\frac{\partial\sigma_{jz}^{(1)}}{\partial x}\right|_{x=0}-\left.\frac{\partial\sigma_{jz}^{(2)}}{\partial x}\right|_{x=0}=0,\\&j=x,y.\end{aligned} \tag{46}$$

The first equation in (46) ensures elimination of the discontinuity, while the second equation in (46) ensures a smooth transition of stress components through the interface.

Omitting intermediate calculations, we give here only the final results. The gradient solution [in units of $\mu_1 b_z/(2\pi)$] reads [161,162], for medium1

$$\begin{aligned}\sigma_{xz}^{(1)}&=\sigma_{xz}^{0(1)}+\frac{y}{\sqrt{c_1 r_-}}K_1\left(\frac{r_-}{\sqrt{c_1}}\right)+\int_0^{+\infty}\frac{s\sin(sy)}{\lambda_1+\lambda_2}\\&\quad\times e^{-x\lambda_1}\left[\frac{\lambda_1-\lambda_2}{\lambda_1}e^{-x's}+2\frac{\Gamma-1}{\Gamma+1}e^{-x's}\right]ds,\\\sigma_{yz}^{(1)}&=\sigma_{yz}^{0(1)}-\frac{x-x'}{\sqrt{c_1 r_-}}K_1\left(\frac{r_-}{\sqrt{c_1}}\right)-\int_0^{+\infty}\frac{\lambda_1\cos(sy)}{\lambda_1+\lambda_2}\\&\quad\times e^{-x\lambda_1}\left[\frac{\lambda_1-\lambda_2}{\lambda_1}e^{-x's}+2\frac{\Gamma-1}{\Gamma+1}e^{-x's}\right]ds,\end{aligned} \tag{47}$$

where $\lambda_i=\sqrt{s^2+1/c_i}$, $i=1,2$, and for medium 2

$$\begin{aligned}\sigma_{xz}^{(2)}&=\sigma_{xz}^{0(2)}+2\int_0^{+\infty}\frac{s\sin(sy)}{\lambda_1+\lambda_2}\\&\quad\times e^{x\lambda_2}\left[e^{-x'\lambda_1}+\frac{\Gamma-1}{\Gamma+1}e^{-x's}\right]ds,\\\sigma_{yz}^{(2)}&=\sigma_{yz}^{0(2)}+2\int_0^{+\infty}\frac{\lambda_2\cos(sy)}{\lambda_1+\lambda_2}\\&\quad\times e^{x\lambda_2}\left[e^{-x'\lambda_1}+\frac{\Gamma-1}{\Gamma+1}e^{-x's}\right]ds.\end{aligned} \tag{48}$$

Let us discuss briefly the structure of the gradient solution (47)-(48). First, all stress components contain the classical solution given by (41) and (42), and extra gradient terms in agreement with the theorem of Ru and Aifantis [23,166]. Second, they contain the gradient solution (see Section 2.1.1 and formulas $(2)_{5,6}$ and $(8)_{5,6}$) obtained in [26] for the case of homogeneous medium ($\Gamma=1$, $c_1=c_2=c$) which is represented in a closed analytical form in (47), and in an integral form in (48). When $\Gamma=1$ and $c_1=c_2=c$, it can be shown that (47) and (48) are reduced to the sum of $(2)_{5,6}$ and $(8)_{5,6}$. Third, they contain specific extra gradient terms caused only by the difference in the gradient moduli $c_1$ and $c_2$. These terms are given in integral form by the last terms in (47) and (48) when $\Gamma=1$.

Thus, one can consider separately a 'purely elastic' interface ($\Gamma\neq1$, $c_1=c_2=c$), a 'purely gradient' interface ($\Gamma=1$, $c_1\neq c_2$), as well as a general 'mixed gradient elastic' interface ($\Gamma\neq1$, $c_1\neq c_2$). This has been done in [161,162] and reproduced in [11,160]. Here we restrict our consideration to some formulas and graphical illustrations of the gradient solution.

For example, in the case of a 'purely elastic' interface ($\Gamma\neq1$, $c_1=c_2=c$), the gradient solution is [in units of $\mu_1 b_z/(2\pi)$]

$$\begin{aligned}\sigma_{xz}^{(1,2)}&=\sigma_{xz}^{0(1,2)}+\frac{y}{\sqrt{cr_-}}K_1\left(\frac{r_-}{\sqrt{c}}\right)\\&\quad+\frac{\Gamma-1}{\Gamma+1}\int_0^{+\infty}\frac{s}{\lambda}\sin(sy)e^{-|x|\lambda-x's}ds,\\\sigma_{yz}^{(1,2)}&=\sigma_{yz}^{0(1,2)}-\frac{x-x'}{\sqrt{cr_-}}K_1\left(\frac{r_-}{\sqrt{c}}\right)\\&\quad-\frac{\Gamma-1}{\Gamma+1}\operatorname{sgn}(x)\int_0^{+\infty}\cos(sy)e^{-|x|\lambda-x's}ds,\end{aligned} \tag{49}$$

where $\lambda = \sqrt{s^2 + 1/c}$. Both components are continuous at the interface, in contrast to the classical solution (41)-(42) where $\sigma^0_{yz}$ suffers a jump given by (43). This difference is illustrated in Fig. 9. It is seen that the classical and gradient solutions coincide far ($r > 5\sqrt{c}$) from the interface or the dislocation line, while they are quite different at nanoscopic distances from them ($r < 5\sqrt{c}$). Also, as in a homogeneous medium, the gradient solution is finite at the dislocation line, while the classical one is singular there.

Let us consider now the 'image' force $F_x$ which acts on the dislocation unit length due to the interface (Fig. 8). In the general case of a 'mixed gradient elastic' interface, the gradient solution [in units of $\mu_1 b_z^2/(2\pi)$] reads

$$F_x(x') = b_z\sigma^{(1)}_{yz}(x = x', y = 0) = \frac{\Gamma-1}{\Gamma+1}\frac{1}{2x'} - \int_0^{+\infty}\frac{\lambda_1}{\lambda_1+\lambda_2}\left[\frac{\lambda_1-\lambda_2}{\lambda_1}e^{-2x'\lambda_1} + 2\frac{\Gamma-1}{\Gamma+1}e^{-x'(\lambda_1+s)}\right]ds, \quad (50)$$

where the first term is the classical singular solution and the integral is the extra gradient term. The numerical evaluation of (50) is presented for a 'purely elastic' interface in Fig. 10a, for a 'purely gradient' interface in Fig. 10b, and for a general 'mixed gradient elastic' interface in Fig. 10c, where also a similar solution for x'< 0 is plotted.

It is seen that for a 'purely elastic' interface, the classical singularity is eliminated from the gradient solutions $F_x = F_x^{(el)}$ which attain maximum values at a distance $\approx\sqrt{c}$ from the interface and tend to zero at the interface. This result is especially instructive for the case of a free surface when $\Gamma = 0$ (see the negative-valued curves in Fig. 10a). In fact, there is no image force when the dislocation lies at the free surface, the force emerges and increases when the dislocation begins to penetrate into the material (the estimated dislocation core radius is $\approx 4\sqrt{c}$ [29]), achieves a maximum value and decreases when the dislocation moves inside the material. The last stage is also well described by the classical solution (Fig. 10a) which, however, can not describe at all the abovementioned preceding stages. Within the gradient theory of (4), one can estimate a maximum shear stress $\tau_{max} = |F_x|_{max}/b_z$ which the screw dislocation has to overcome for penetrating into the material. From Fig. 10a, it is estimated that $\tau_{max} \approx \mu/(2\pi)$, i.e. the value of theoretical shear strength [5]. For the case of two bonded solids, the result of zero value at the interface (i.e., the appearance of an unstable equilibrium position there) is not as clear.

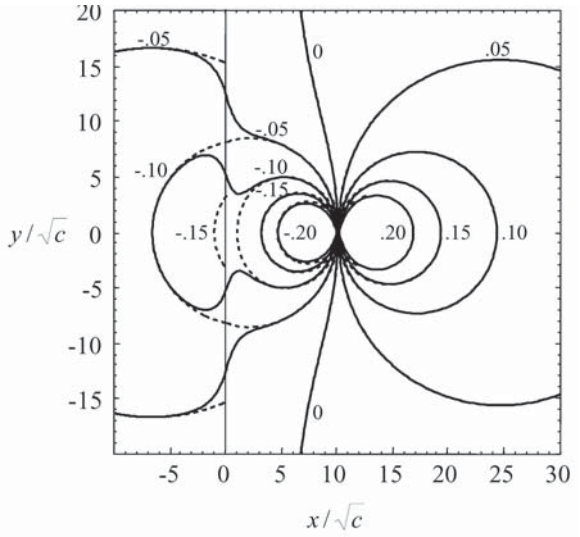


**Fig. 9.** Stress field $\sigma_{yz}$ map for a screw dislocation located at the point (10,0) near a flat interface (at x = 0) separating two elastic media with $\mu_2 = 2\mu_1$ and $c_1 = c_2 = c$. The stresses are given in units of $\mu_1 b_z/(2\pi\sqrt{c})$. The dashed contours represent the classical solution $\sigma^0_{yz}$.

In the case of a 'purely gradient' interface, the 'image' force acts upon the dislocation due to the difference in the gradient coefficients $c_1$ and $c_2$, and is given by (50) with $\Gamma = 1$. When $c_1 > c_2$, i.e. $\lambda_1 < \lambda_2$, the integral in (50) is negative and the force $F_x = F_x^{(gr)}$ is positive. This means that the dislocation is pushed away from the interface into the bulk of material 1 which has the larger gradient coefficient. Plots for $F_x^{(gr)}(x')$ are presented in Fig. 10b from which one can conclude that this force has a short-range character and acts just near the interface. At the interface, it attains a maximum value which depends strongly on the ratio $c_2/c_1$.

In the general case of a 'mixed gradient elastic' interface, the gradient solution for $F_x$ described by (50) is not a simple superposition of $F_x^{(el)}$ and $F_x^{(gr)}$. However, it manifests their characteristic features (Fig. 10c). Similar to $F_x^{(el)}$, the general force $F_x$ is a nonsingular long-range force which coincides with the classical solution far ($|x'| > 5\sqrt{c_1}$) from the interface. Similar to $F_x^{(gr)}$, it attains non-zero values at

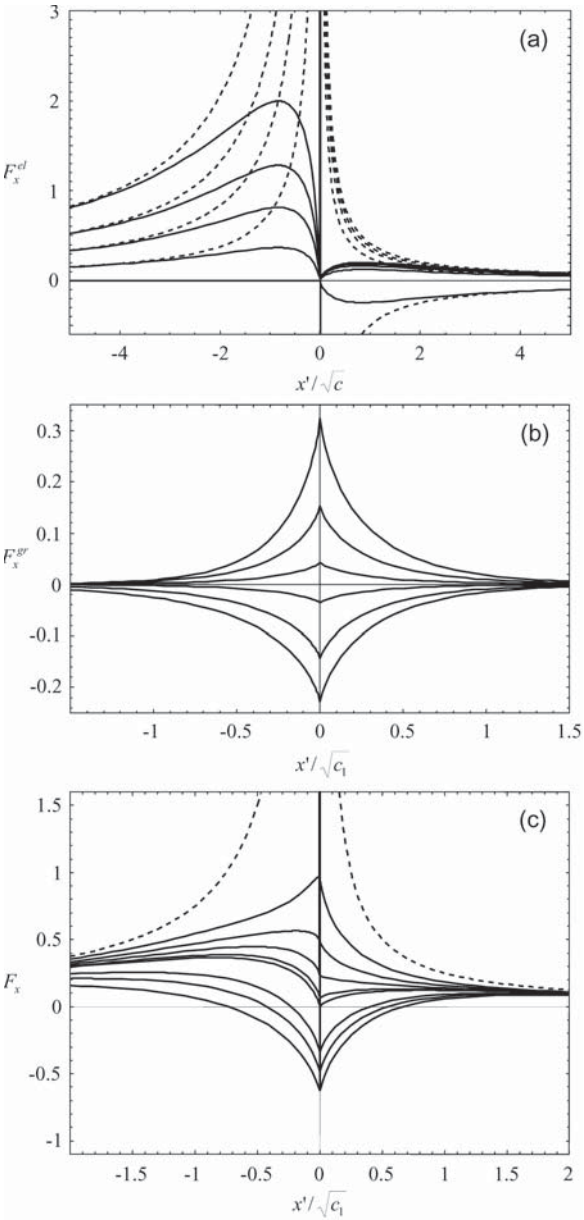


**Fig. 10.** The "image" force which acts upon the dislocation unit length due to the interface (at x' = 0) of two elastic media as a function of the dislocation position. (a) Purely elastic interface with $c_1 = c_2 = c$ and $\mu_2/\mu_1$ = 10, 7, 5, 3 and 0 (from top to bottom). (b) Purely gradient interface with $\mu_1 = \mu_2$ and $c_2/c_1$ = 0.5, 0.7, 0.9, 1.1, 1.5 and 2 (from top to bottom). (c) Mixed elastic and gradient interface with $\mu_2 = 3\mu_1$ and $c_2/c_1$ = 0.3, 0.5, 0.7, 0.9, 1, 2, 3 and 5 (from top to bottom). The force values are given in units of $\mu_1 b_z^2/(2\pi\sqrt{c_1})$. The dashed curves represent the classical solution.

the interface which depend on both ratios $\mu_2/\mu_1$ and $c_2/c_1$. In fact, the sign and qualitative behavior of $F_x$ near the interface is entirely determined by $c_2/c_1$. For example, if $\mu_2>\mu_1$, there are three different types of behavior of $F_x$. When $c_2< c_1$, $F_x > 0$ everywhere and attains maximum values near or at the interface. When $c_2 = c_1$, $F_x \equiv F_x^{(el)}$ and becomes equal to zero at the interface. When $c_2>c_1$, $F_x > 0$ except at a small region around the interface. The size of this region which depends on $c_2/c_1$ is about $\sqrt{c_1}$, and $F_x<0$ inside this region attaining its minimum value at the interface. When $c_2<c_1$, the dislocation is pushed from material 2 into material 1 and has no equilibrium position. When $c_2 = c_1$, it does the same but it has an unstable equilibrium position at the interface. When $c_2 > c_1$, a dislocation being in material 2, is attracted to the interface and is locked at a stable equilibrium position $x' \approx -(0.2...0.8)\sqrt{c_1}$ near that interface, while a dislocation located in material 1, has an unstable equilibrium position $x' \approx (0.4...0.7)\sqrt{c_1}$ near the interface; being attracted to it within a small region $x' < (0.4...0.7)\sqrt{c_1}$ and pushed away from it otherwise.

One can summarize that within the gradient elasticity theory described by (4), both non-vanishing stress components of a screw dislocation remain continuous at the interface, in contract to the well-known classical solution (41)-(42) having a component which undergoes a jump discontinuity there. Far from the interface and the dislocation lines (at distances $>>10\sqrt{c_1}$), gradient and classical solutions coincide. It has also been dispensed with the classical singularity of the elastic 'image' force acting upon a dislocation due to the interface, and shown that this force remains finite there. In fact, an additional short-range elastic interaction between the dislocation and the interface due to a difference in the gradient coefficients of the media in contact has appeared. The appropriate additional 'image' force acting upon the dislocation, is finite and maximum at the interface. Under the action of this force, the dislocation tends to penetrate into the medium having the larger gradient coefficient. In the general case where both the elastic constants $\mu_i$ and the gradient coefficients $c_i$ are different for the bonded media, the total 'image' force manifests quite different behavior near the interface depending on the ratios $\mu_2/\mu_1$ and $c_2/c_1$, while its long-range component remains as in the classical theory of elasticity.

### 3.1.1.2. Edge dislocation

The classical solution for an *edge* dislocation shown in Fig. 11 is given (in units of $\mu_1/[\pi(k_1+1)]$) in medium 1 by [152]

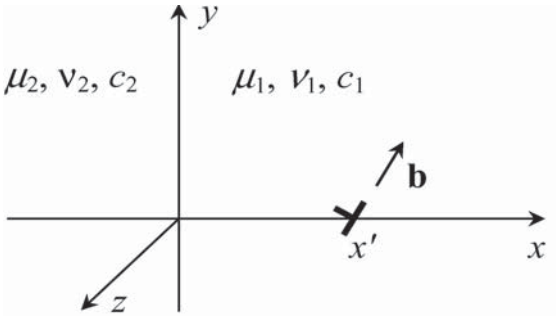


**Fig. 11.** Edge dislocation near a flat interface between the materials having different shear moduli $\mu_1$ and $\mu_2$, Poisson ratios $\nu_1$ and $\nu_2$, and different gradient coefficients $c_1$ and $c_2$.

$$\sigma_{xx}^{0(1)} = b_x\left\{-\frac{2y}{r_-^2}-\frac{4yx_-^2}{r_-^4}+\frac{(A+B)y}{r_+^2}+\frac{4Ay\left(x'^2+x^2\right)}{r_+^4}+\frac{32Ayxx'x_+^2}{r_+^6}\right\}$$
$$+b_y\left\{-\frac{2x_-}{r_-^2}+\frac{4x_-^3}{r_-^4}+\frac{(A+B)x-(3A-B)x'}{r_+^2}+\frac{4Ax_+\left(x'^2-6x'x-x^2\right)}{r_+^4}+\frac{32Axx'x_+^3}{r_+^6}\right\},$$
$$\sigma_{yy}^{0(1)} = b_x\left\{-\frac{2y}{r_-^2}+\frac{4yx_-^2}{r_-^4}+\frac{(3A-B)y}{r_+^2}+\frac{4Ay\left(3x'^2+4x'x-x^2\right)}{r_+^4}-\frac{32Ayxx'x_+^2}{r_+^6}\right\}$$
$$+b_y\left\{\frac{6x_-}{r_-^2}-\frac{4x_-^3}{r_-^4}-\frac{(5A+B)x+(9A+B)x'}{r_+^2}+\frac{4Ax_+\left(3x'^2+10x'x+x^2\right)}{r_+^4}-\frac{32Axx'x_+^3}{r_+^6}\right\},$$
$$\sigma_{xy}^{0(1)} = b_x\left\{-\frac{2x_-}{r_-^2}+\frac{4x_-^3}{r_-^4}+\frac{(3A-B)x-(A+B)x'}{r_+^2}+\frac{4Ax_+\left(x'^2+6x'x-x^2\right)}{r_+^4}-\frac{32Axx'x_+^3}{r_+^6}\right\} \qquad (51)$$
$$+b_y\left\{-\frac{2y}{r_-^2}+\frac{4yx_-^2}{r_-^4}+\frac{(A+B)y}{r_+^2}-\frac{4Ay\left(x'^2+4x'x+x^2\right)}{r_+^4}+\frac{32Ayxx'x_+^2}{r_+^6}\right\},$$
$$\sigma_{zz}^{0(1)} = \nu_1\left[\sigma_{xx}^{0(1)}+\sigma_{yy}^{0(1)}\right],$$

and in medium 2 by

$$\sigma_{xx}^{0(2)} = b_x\left\{\frac{(A+B-2)y}{r_-^2}-\frac{4yx_-\left[(1-B)x-(1-A)x'\right]}{r_-^4}\right\}$$
$$+b_y\left\{\frac{(A+B-2)x+(B-3A+2)x'}{r_-^2}+\frac{4x_-^2\left[(1-B)x-(1-A)x'\right]}{r_-^4}\right\},$$
$$\sigma_{yy}^{0(2)} = b_x\left\{\frac{(3B-A-2)y}{r_-^2}+\frac{4yx_-\left[(1-B)x-(1-A)x'\right]}{r_-^4}\right\}$$
$$+b_y\left\{\frac{(6-5B-A)x+3(B+A-2)x'}{r_-^2}-\frac{4x_-^2\left[(1-B)x-(1-A)x'\right]}{r_-^4}\right\},$$
$$\sigma_{xy}^{0(2)} = b_x\left\{\frac{(3B-A-2)x+(2-A-B)x'}{r_-^2}+\frac{4x_-^2\left[(1-B)x-(1-A)x'\right]}{r_-^4}\right\} \qquad (52)$$
$$+b_y\left\{\frac{(A+B-2)y}{r_-^2}+\frac{4yx_-\left[(1-B)x-(1-A)x'\right]}{r_-^4}\right\},$$
$$\sigma_{zz}^{0(2)} = \nu_2\left[\sigma_{xx}^{0(2)}+\sigma_{yy}^{0(2)}\right],$$

where $x_{\pm} = x \pm x'$, $r_{\pm}^2 = x_{\pm}^2 + y^2$, $A = (1 - \Gamma)/(1 + k_1\Gamma)$, $B = (k_2 - k_1\Gamma)/(k_2 + \Gamma)$, $k_i = 3 - 4\nu$, $i = 1,2$.

It is easily seen that the components $\sigma_{xx}^0$ and $\sigma_{xy}^0$ are continuous across the interface ($x = 0$), while the components $\sigma_{yy}^0$ and $\sigma_{zz}^0$ suffer jump discontinuities $[\sigma_{kl}^0] = \sigma_{kl}^{0(1)} - \sigma_{kl}^{0(2)}$ there which (in units of $\mu_1/[\pi(1-\nu_1)]$) are given by

$$\begin{aligned}
\left[\sigma_{yy}^0\right]_{x=0} &= \frac{(A-B)b_x y - (3A+B)b_y x'}{x'^2 + y^2} + \frac{4A\left(b_x y + b_y x'\right)x'^2}{\left(x'^2 + y^2\right)^2}, \\
\left[\sigma_{zz}^0\right]_{x=0} &= \frac{\nu_1\left[(A-1)b_x y - (3A+1)b_y x'\right] - \nu_2(B-1)\left(b_x y + b_y x'\right)}{x'^2 + y^2} \\
&\quad + \frac{4\nu_1 A\left(b_x y + b_y x'\right)x'^2 - 2\nu_2(A-1)b_y x'^3}{\left(x'^2 + y^2\right)^2}.
\end{aligned} \tag{53}$$

As discussed in detail above, such jumps are to be expected from the macroscopic viewpoint of classical elasticity, but they may not be justifiable from a nanoscopic point of view. We have concluded that stress jumps like those in (53) is a consequence of the approximation of classical continuum models which often become inadequate for the description of nanoscale phenomena. To demonstrate this fact, we note that the stress jumps in (53) tend to infinity in the *xz*-plane when the dislocation approaches the interface. It follows again that the interface stress jumps have to be eliminated from the solution of this problem within any generalized theory of elasticity aiming to consider nanoscale phenomena.

To solve the problem under consideration within the gradient theory described by (4), one has to find the solution of inhomogeneous Helmholtz equation (44) with the classical boundary conditions

$$\left[\sigma_{xx}\right]_{x=0} = \left[\sigma_{xy}\right]_{x=0} = 0 \tag{54}$$

and six extra boundary conditions [163]

$$\begin{aligned}
&\left[\sigma_{yy}\right]_{x=0} = \left[\sigma_{zz}\right]_{x=0} = 0, \\
&\left[\frac{\partial\sigma_{xx}}{\partial x}\right]_{x=0} = \left[\frac{\partial\sigma_{yy}}{\partial x}\right]_{x=0} = \left[\frac{\partial\sigma_{xy}}{\partial x}\right]_{x=0} = \left[\frac{\partial\sigma_{zz}}{\partial x}\right]_{x=0} = 0.
\end{aligned} \tag{55}$$

The last four equations in (55) ensure the smooth transition of stress components across the interface.

Eq. (44) with right-hand parts (51)-(52) and boundary conditions (54)-(55) was solved and discussed in detail by Mikaelyan *et al.* [163] (see also [11,160]). The gradient solution is written as the sum $\sigma_{kl}^{(i)} = \sigma_{kl}^{0(i)} + \sigma_{kl}^{gr(i)}$, where $\sigma_{kl}^{0(i)}$ are given by (51)-(52) and $\sigma_{kl}^{gr(i)}$ are the extra gradient terms. The stress components $\sigma_{kl}^{(i)}$ (we do not show them here because they are rather cumbersome) are continuous across the interface ($x = 0$). When $\mu_1 = \mu_2 = \mu$, $\nu_1 = \nu_2 = \nu$, and $c_1 = c_2 = c$ (the case of a homogeneous medium), they are reduced into the gradient solution obtained in [26]. When $c_1 = c_2 \to 0$ (the limiting transition to the classical elasticity), the extra gradient terms disappear.

As is the case with screw dislocation, here we can also consider separately a 'purely elastic' interface ($\mu_1 \neq \mu_2$, $\nu_1 \neq \nu_2$, $c_1 = c_2 = c$), a 'purely gradient' interface ($\mu_1 = \mu_2$, $\nu_1 = \nu_2$, $c_1 \neq c_2$), as well as a general 'mixed gradient elastic' interface ($\mu_1 \neq \mu_2$, $\nu_1 \neq \nu_2$, $c_1 \neq c_2$).

For example, in the first case, we consider the effects caused only by the difference in the elastic constants of the bonded media. Two main advantages of the gradient solution may be pointed out in this connection. First, there are no singularities in the stress components $\sigma_{kl}^{(i)}$ at the dislocation line. Second, there are no jumps like those given by (53) in $\sigma_{yy}^{(i)}$ and $\sigma_{zz}^{(i)}$ at the interface. This allows one to consider nanoscale short-range elastic interactions between dislocations and interfaces, in contrast to the classical singular solution (51)-(52) where these components suffer jump discontinuities at the interface. This is illustrated in Fig. 12 for the component $\sigma_{yy}^{(i)}(x,0)$ of a dislocation with Burgers vector $\mathbf{b} = b_y\mathbf{e}_y$. It is seen that classical and gradient solutions coincide far ($r > 10\sqrt{c}$) from the interface or the dislocation line, while near them (within nanoscopic distances $r < 10\sqrt{c}$) they are quite different.

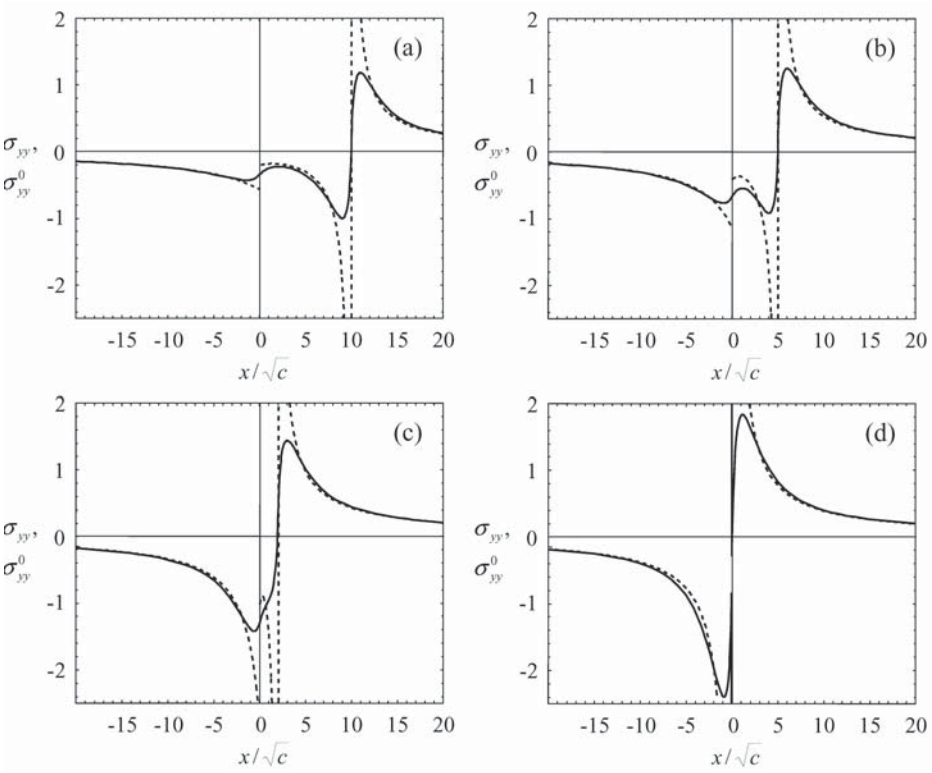


**Fig. 12.** The stress component $\sigma_{yy}(x,y = 0)$ near the line of an edge dislocation with the Burgers vector $\mathbf{b} = b_y\mathbf{e}_y$ located at distances $x'/\sqrt{c}$ = 10 (a), 5 (b), 2 (c), and 0 (d) from the interface (at x = 0) of two elastic media with $\mu_2 = 10\mu_1$, $\nu_1 = \nu_2 = 0.3$ and $c_1 = c_2 = c$. The stress values are given in units of $\mu_1 b_y/(\pi(k_1+1)\sqrt{c})$. The dashed curves represent the classical solution $\sigma^0_{yy}$.

Let us consider now the 'image' force $F_x$ which acts upon the dislocation unit length by the interface (Fig. 11). For a dislocation with Burgers vector $\mathbf{b} = b_x\mathbf{e}_x$, the gradient solution $F_x(x') = b_x\sigma^{(1)}_{xy}(x = x',0)$ reads (in units of $\mu_1 b_x^2/[\pi(k_1+1)]$) [163]

$$F_x(x') = -\frac{A+B}{2x'} + \frac{4Ac_1}{x'^3} + 4\int_0^{+\infty} \frac{s}{\lambda_1+\lambda_2} \times\Big[c_1 s(\lambda_1-\lambda_2)e^{-2x'\lambda_1} + \big\{B - Ac_1(\lambda_1^2+\lambda_2 s) \times(1+2x's) - c's(\lambda_2 - s)\big\}e^{-x'(\lambda_1+s)}\Big]ds, \quad (56)$$

where $c' = c_1 + c_2(B - 1)$. The first term in (56) is the classical singular solution and the others are the extra gradient terms. The numerical evaluation of (56) is presented for a 'purely elastic' interface in Fig. 13a, for a 'purely gradient' interface in Fig. 13b, and for a general 'mixed gradient elastic' interface in Fig. 13c, where also a similar solution for $x' < 0$ is plotted.

It is seen that for a 'purely elastic' interface, the classical singularity is eliminated from the gradient solutions $F_x = F_x^{(el)}$ which attain maximum values at a distance $\approx\sqrt{c}$ from the interface and has no jumps at the interface. In the case of a free surface when $\mu_2 = \nu_2 = 0$ (see the negative-valued curves in Fig. 13a), there is no image force when the dislocation lies at the free surface. The force appears and increases when the dislocation begins to penetrate into the material, achieves a maximum value and decreases when the dislocation moves inside the material as is the case with a screw dislocation. A maximum shear stress $\tau_{max} = |F_x|_{max}/b_z$, which the edge dislocation has to overcome for penetrating into the material, is estimated as $\tau_{max} \approx \mu/(2.8\pi)$ (for $\nu = 0.3$), i.e. the value of theoretical shear strength [5].

In the case of a 'purely gradient' interface, the 'image' force acts upon the dislocation due to the difference in the gradient coefficients $c_1$ and $c_2$, and is given by (56) with $\mu_1 = \mu_2$ and $\nu_1 = \nu_2$. A numerical evaluation of (56) shows that the force $F_x = F_x^{(gr)}$ is

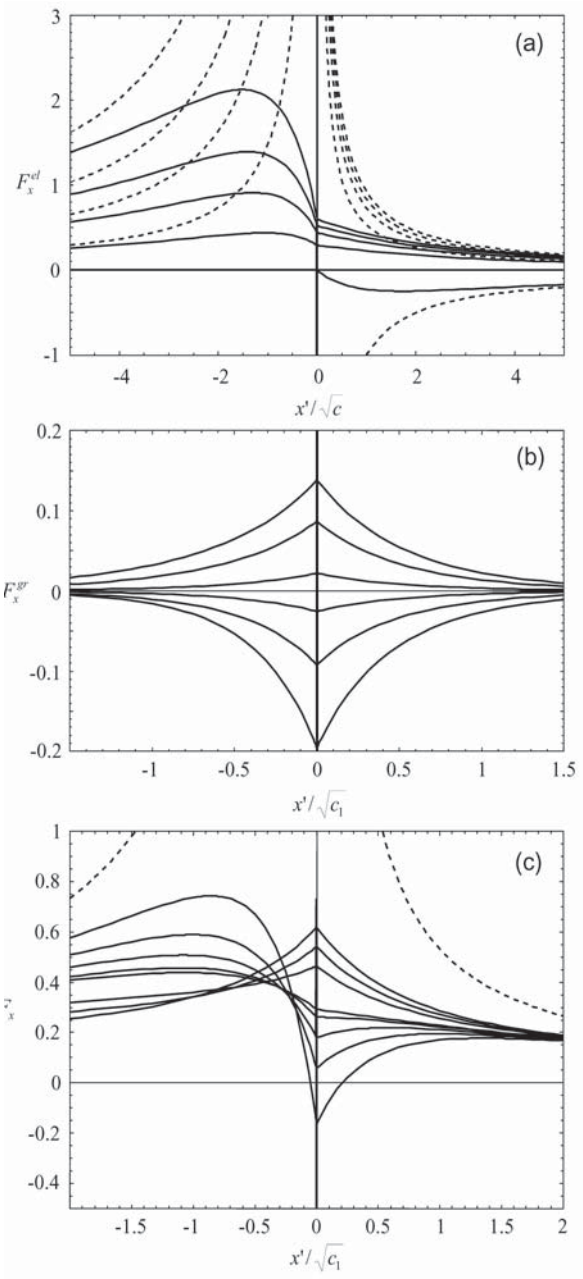


**Fig. 13.** The 'image' force which acts upon the dislocation unit length due to the interface (at $x'$ = 0) of two elastic media as a function of the dislocation position. (a) Purely elastic interface with $c_1 = c_2 = c$ and $\mu_2/\mu_1$ = 10, 7, 5, 3 and 0 (from top to bottom). (b) Purely gradient interface with $\mu_1 = \mu_2$ and $c_2/c_1$ = 2, 1.5, 1.1, 0.9, 0.7 and 0.5 (from top to bottom). (c) Mixed elastic and gradient interface with $\mu_2 = 3\mu_1$ and $c_2/c_1$ = 5, 3, 2, 1, 0.9, 0.7, 0.5 and 0.3 (from top to bottom). The force values are given in units of $\mu_1 b_x^2/[\pi(k_1+1)\sqrt{c_1}]$, $\nu_1 = \nu_2 = 0.3$. The dashed curves represent the classical solution.

positive when $c_1 < c_2$ and negative when $c_1 > c_2$ (Fig. 13b). This means that an edge dislocation is pushed away from the interface into the bulk of the material which has the smaller gradient coefficient, in contrast to the case of a screw dislocation which exhibits opposite behavior. The reasons for this difference are not clear as yet. From Fig. 13b, one can conclude that the dependence $F_x^{(gr)}(x')$ has a short-range character and this force acts just near the interface. At the interface, it attains a maximum value which depends strongly on the ratio $c_2/c_1$.

In the general case of a 'mixed gradient elastic' interface, the gradient solution for $F_x$ described by (56) is not a simple superposition of $F_x^{(el)}$ and $F_x^{(gr)}$ as is illustrated in Fig. 13c. The general force $F_x$ is a nonsingular long-range force which is continuous across the interface and coincides with the classical solution far ($|x'|>5\sqrt{c_1}$) from the interface. Its value at the interface depends strongly on both ratios $\mu_2/\mu_1$ and $c_2/c_1$. In fact, the sign and qualitative behavior of $F_x$ near the interface may be determined by $c_2/c_1$. For example, for $\mu_2 = 3\mu_1$, there are three different types of behavior for $F_x$ (Fig. 13c). When $c_1 < c_2$, $F_x > 0$ everywhere and attains maximum values near or at the interface. When $c_1 = c_2$, $F_x \equiv F_x^{(el)}$ (see above). When $c_1 > c_2$, $F_x > 0$ except at a small region around the interface. Its size depends on $c_2/c_1$ and is about $0.3\sqrt{c_1}$; $F_x < 0$ inside this region and attains minimum values at the interface. Thus, when $c_1 \le c_2$, the dislocation is pushed from material 2 into material 1 and possesses no equilibrium position. When $c_1 > c_2$ (e.g. $c_2 = 0.3c_1$), a dislocation being in material 2, is attracted to the interface and may be locked at a stable equilibrium position $x' \approx -0.1\sqrt{c_1}$ near that interface, while a dislocation located in material 1, possesses an unstable equilibrium position $x' \approx 0.2\sqrt{c_1}$ near the interface; being attracted to it within a small region $x' < 0.2\sqrt{c_1}$ and pushed away from it otherwise.

Thus, within the gradient elasticity theory described by (4), all stress components of an edge dislocation remain continuous at the interface, in contract to the well-known classical solution (51)-(52) where two normal stress components suffer jump discontinuities there. Far from the interface and the dislocation lines (at distances $>>10\sqrt{c_1}$), gradient and classical solutions coincide. It has also been dispensed with the classical singularity of the elastic 'image' force acting upon a dislocation due to the interface, and shown that this force remains finite and continuous throughout. An additional short-range elastic interaction between the dislocation and the interface due to a difference in the gradient co-

efficients of the media in contact has appeared. The appropriate additional 'image' force acting upon the dislocation, is finite and maximum at the interface. Under the action of this force, the dislocation tends to penetrate into the medium with the smaller gradient coefficient (in contrast to the just opposite situation with a screw dislocation). In the general case where both the elastic constants $\mu_i$ and the gradient coefficients $c_i$ are different for the bonded media, the total 'image' force exhibits quite different behavior near the interface depending on the ratios $\mu_2/\mu_1$ and $c_2/c_1$, while its long-range component remains as in the classical theory of elasticity.

Here, as practically always, we have not considered the effect of elastic anisotropy. The description of defects within the anisotropic theory of elasticity is more complicated technically and occurs very cumbersome. It is enough to say that the elastic behavior of straight dislocations parallel to flat outer or internal boundaries in various anisotropic media has been studied during almost 45 years [167-195]. At the same time, in modeling plastic deformation, the errors due to use of isotropic solutions instead of anisotropic ones usually do not exceed one or two tens per cent. That is why, in reviewing the existing solutions of boundary-value problems for defects, we only note the works where these problems have been studied with account for elastic anisotropy but do not discuss them in detail.

It is also worth noting that Head [165] and Chen et al. [196] considered the behavior of dislocations near flat slipping interfaces. However, these results have not been used broadly in applications until now.

### 3.1.2. Straight dislocations piercing flat interfaces

The boundary-value problems of that kind are commonly rather complicated. The most of the solutions are cumbersome even within the classical isotropic theory of elasticity. The field of their application mainly includes theories of dislocation images in polarized light optics, X-ray topography and diffraction, and electron microscopy. We give below a short list of the well-known solutions without pretending to its completeness.

First of all, we set off the works [46,47,154,197-206] devoted to the elastic fields of dislocations crossing a flat free surface of an elastically isotropic solid. Yoffe [197] was the first who considered a mixed straight dislocation intersecting the free surface under an arbitrary angle, and found the displacement fields around this dislocation. Her results were corrected by Shaibani and Hazzledine [198]. Maksimov *et al.* [199,200] obtained an integral form for the distortion fields of inclined dislocations and used this solution in computer simulation of electron-microscopy images for these dislocations. Belov and Chamrov [201] found the other solution (different from that of [197,198] and useful for various applications) for the displacements of an inclined dislocation and utilized it in calculations of electron-microscopy contrast. The force of interaction between a free surface and an inclined dislocation was calculated by Indenbom and Dubnova [202]. Special cases of dislocations perpendicular to a free surface were considered by Eshelby [154] and Honda [203]. More recent calculations by Kolesnikova and Romanov [46,47] improved the stress fields of a screw dislocation represented in review [154], and approved the solution [203] for an edge dislocation. Another screw dislocation solution, given in the form of singular integrals, was obtained by Arias and Lund [204] through a limiting transition from a general solution for a dislocation loop in a finite 3D sample. Note that the displacement and stress fields [198] of a screw dislocation normal to the flat free surface, have been used recently as basic fields for solving a much more complicated boundary-value problem on a cylindrical cavity (micropipe) containing a screw dislocation and perpendicular to the free surface of a crystal [205,206].

The solution for a screw dislocation perpendicular to a flat interface between two elastically isotropic media with different elastic moduli, was found by Hsieh and Dundurs [207] and represented also in review [154].

The account for elastic anisotropy in the problems on dislocations emerging at flat free surfaces or piercing flat interphase boundaries was evaluated by Lothe *et al.* [208-210] and Belov *et al.* [211], respectively. A review of these solutions is given by Belov [212].

### 3.1.3. Dislocation loops near flat interfaces

The first investigation of a general solution for all six Volterra's dislocations (dislocations and disclinations) in an elastically isotropic half-space was carried out by Steketee [213] who obtained the displacement fields in an integral form. Here and in Section 3.2.2 we briefly consider the boundary-value problems solved for the loops of dislocations and

disclinations, respectively, which lie near flat interfaces in infinite and semi-infinite media. The works done to the early 80-ies of the XX century are reviewed in [6,46,154].

One of the most effective methods in calculating the elastic fields of various defects is use of infinitesimal dislocation loops [37]$_2$. Such a loop has the infinitesimal square and is determined by the directions of its infinitesimal Burgers vector and the normal vector to the loop plane. The elastic fields of these loops may play the role of Green's function for the elastic medium. There are a number of boundary-value problems solved for these loops, which may be used for construction of similar solutions for defects (in particular, dislocation loops) of finite sizes. Tikhonov [214] studied the force of interaction between an arbitrary oriented infinitesimal dislocation loop and the free surface of an elastic solid. Groves and Bacon [215,216] found an analytical solution for the field of displacements of such a loop. Vagera [217] calculated the fields of displacements and stresses around an infinitesimal prismatic dislocation loop placed near an perfectly bonded interphase boundary, and the displacement field for the same loop near a slipping interphase boundary. He also determined the force of interaction between the loop and these boundaries. The stress field of an infinitesimal dislocation loop lying near an interphase boundary was also obtained by Salamon and Dundurs [41]. Bonnet [218] considered the elastic fields for an infinitesimal dislocation loop localized at the interface.

A few boundary-value problems were solved for finite-size dislocation loops. The elastic fields of circular loops in a half-space were studied by Вальтескб [219], Gavazza and Barnett [220], Jдger *et al*. [221], and Ohr [222], while in a two-phase material by Salamon and Dundurs [41,223,224], Salamon and Comninou [225], Salamon [226], and Yu and Sanday [227]. The prismatic loops were considered in [41,219-223,225,227], the glide loops in [41,224,226,227]. The loop plane was commonly chosen to be parallel to the interface (to free surface [219-222] or interphase boundary [41,223-226]), or to coincide with the interphase boundary [225,226]. Yu and Sanday [227] obtained the most general solution for an arbitrary orientation of the loop plane, and considered the special cases of prismatic and glide loops near perfectly bonded or slipping interfaces. They checked in passing the limiting cases studied before in [41,223-226], approved the correctness of preceding solutions and corrected a misprint in [226].

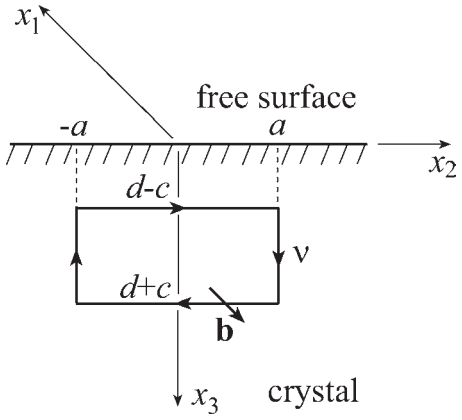


**Fig. 14.** Rectangular prismatic dislocation loop near a free surface.

All of the abovementioned solutions [41,213-227] were found for elastically isotropic solids. The elastic fields of circular dislocation loops in anisotropic two-phase media were considered by Koguchi [228] and Li and Li [229].

For non-smooth dislocation loops, we are aware of only three solutions of appropriate boundary-value problems. Keer and Polonsky [230] obtained a closed analytical solution for the displacement field of a triangle loop placed in an interphase boundary. Rectangular prismatic and glide dislocation loops with planes perpendicular to free surfaces of elastically isotropic solids were recently considered in [58] and [206], respectively. The authors calculated the strain energies of the loops in explicit analytical form and applied them to the models of local plastic deformation near rod-like inclusions (nanowires) [58] and cylindrical cavities (micropipes) [206].

Since these solutions seem to be useful in different applications, we discuss them below in more details.

Consider a rectangular prismatic dislocation loop which lies in the plane $x_1 = 0$ near the flat free surface $x_3 = 0$ of an elastically isotropic half-space and is bounded by the segments $x_2 = \pm a$ and $x_3 = d \pm c$ (Fig. 14). Let the loop Burgers vector be directed against the $x_1$-axis, $\mathbf{b} = -b\mathbf{e}_1$. Following [58], the strain energy of the loop reads (in units of $Db^2/2$)

$$W^{l} = S_1 + 2S_2 + S_3 + \left[3 - 4\nu(3 - 2\nu)\right]S_4 + 2\frac{1 - 2\nu\left(6 - 11\nu + 8\nu^3\right)}{(1 - 2\nu)^2}S_5$$
$$- \frac{129 - 2\nu\{234 - \nu\left[245 - 4\nu(5 + 16\nu)\right]\}}{3(1 - 2\nu)^2}S_6, \qquad (57)$$

where

$$S_1 = a\ln\frac{(\kappa_2 - a)(\kappa_3 + a)^2\left(\sqrt{a^2 + (d - c + r_0/2)^2} - a\right)}{(\kappa_2 + a)(\kappa_3 - a)^2\left(\sqrt{a^2 + (d - c + r_0/2)^2} + a\right)},$$

$$S_2 = a\ln\frac{16a^2(\kappa_4 - a)}{r_0^2(\kappa_4 + a)} + c\ln\frac{16c^2(\kappa_4 - c)}{r_0^2(\kappa_4 + c)} - 4(a + c - \kappa_4),$$

$$S_3 = \frac{8(1 - \nu)(1 - 2\nu)c^2 d}{a^2} + \frac{3c^2}{d} - \frac{2c^2(a^2 + d^2)\kappa_3}{a^2 d^2},$$

$$S_4 = \frac{2d^2\kappa_3 - (d - c)^2\kappa_1 - (d + c)^2\kappa_2}{2a^2}, \qquad (58)$$

$$S_5 = c\ln\frac{(d + c)(d - c + \kappa_1)}{(d - c)(d + c + \kappa_2)} + d\ln\frac{(d^2 - c^2)(d + \kappa_3)}{d(d - c + \kappa_1)(d + c + \kappa_2)},$$

$$S_6 = 2\kappa_3 - \kappa_1 - \kappa_2$$

and $\kappa_{1,2}^2 = a^2 + (d \mp c)^2$, $\kappa_3^2 = a^2 + d^2$, $\kappa_4^2 = a^2 + c^2$.

Let us check some important limiting cases. In the limiting case $d \to \infty$ these formulas are transformed into formula (17) for the strain energy of such a loop in an infinite medium.

When $a \to \infty$, the strain energy of the dislocation loop, divided by $2a$, transforms into the strain energy (per unit length) $w_{\parallel}^{dip}$ of a dipole of edge dislocations which are parallel to the free surface:

$$w_{\parallel}^{dip} = \lim_{a\to\infty}\frac{W^{l}}{2a} = \frac{Db^2}{2}\left[\ln\frac{d - c + r_0/2}{r_0/2} + \ln\frac{d + c}{r_0/2} - 2\ln\frac{d}{c} - \frac{c^2}{d^2}\right]. \qquad (59)$$

For $c \to \infty$, the strain energy of the dislocation loop, divided by $2c$, is equal to the strain energy $w_{\perp}^{dip}$ of a dipole of edge dislocations (per their unit length) whose lines are perpendicular to the free surface:

$$w_{\perp}^{dip} = \lim_{c\to\infty}\frac{W^{l}}{2c} = Db^2\ln\frac{2a}{r_0}. \qquad (60)$$

This formula coincides with that for strain energy of a similar dislocation dipole in an infinite medium [5].

Dependences of the energy $W^{l}$ on the interspacing $d$ between the centre of the dislocation loop and the free surface are shown in Fig. 15, for $c = 10b$, $r_0 = b$, $\nu = 0.3$ and different values of $a$ [58]. As follows from Fig. 15, the energy $W^{l}$ decreases with rising $d$ at low values of $a/c$ (for example, see curve 1 with $a = c/2$). When the ratio $a/c$ increases, the dependence $W^{l}(d)$ exhibits a maximum $W^{l} = W_{\max}^{l}$ at some $d$ (see curve 2 with $a = c$). At high values of $a/c$, the height $W_{\max}^{l} - W_{\infty}^{l}$, where $W_{\infty}^{l} = W^{l}(d \to \infty)$, of the maximum decreases (see curves 3 and 4 with $a = 2c$ and $4c$, respectively) and approaches zero in the limit of $a \to \infty$ (see curve 5).

Let us consider similar problems for two rectangular glide dislocation loops having Burgers vectors perpendicular (Fig. 16a) or parallel (Fig. 16b) to the free surface. As shown in [206], the strain energy $W^{l(1)}$ of the first loop is given by

$$W^{l(1)} = \frac{Db^2}{4}\left\{(2-\nu)(\bar{R}_1 - \bar{R}_2)\right.$$
$$+\left(\frac{2x_3x_3'}{(x_3+x_3')^2} + \frac{4(1-\nu)x_3'}{x_3+x_3'}\right)\bar{R}_2$$
$$-\bar{x}_2 \ln\frac{\bar{x}_2+\bar{R}_1}{\bar{x}_2+\bar{R}_2} - (1-\nu)\left[(x_3'-x_3)\left(\frac{2\bar{R}_2}{x_3+x_3'}\right.\right.$$
$$\left.+\ln\frac{x_3'-x_3+\bar{R}_1}{(x_3'+x_3+\bar{R}_2)^2}\right) + \left[(5-8\nu)(x_3+x_3')\right. \qquad (61)$$
$$\left.\left.\left.-4x_3'\right]\ln(x_3+x_3'+\bar{R}_2)\right]\right\}\Bigg|_{x_2'=0}^{2a}\Bigg|_{x_3'=d-c}^{d+c}\Bigg|_{x_2=r_0}^{2a-r_0}\Bigg|_{x_3=d-c+r_0}^{d+c-r_0},$$

where $\bar{x}_2 = x'_2 - x_2$ and $\bar{R}_{1,2} = \bar{x}_2^2 + (x_3 \mp x_3')^2$. In the limiting case $d \to \infty$ formula (61) is transformed into formula (19) for the strain energy of a glide dislocation loop in an infinite medium. When $a \to \infty$, the strain energy (61), divided by $2a$, transforms into the strain energy (59) of a dipole of edge dislocations which are parallel to the free surface. For $d = c \to \infty$, the strain energy of the dislocation loop, divided by $2c$, is equal to the strain energy $w_\perp^{dip(1)}$ of a dipole of screw dislocations (per their unit length) whose lines are perpendicular to the free surface. For $r_0 << a$, $w_\perp^{dip(1)}$ is as follows:

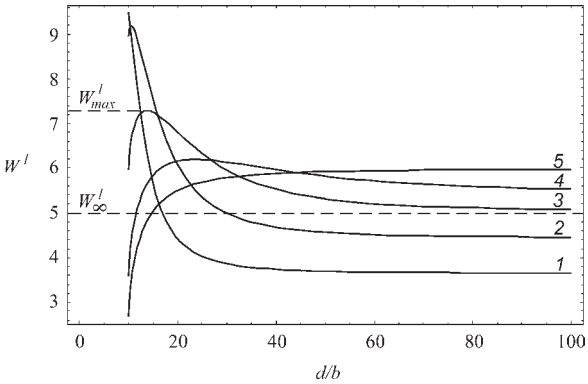


**Fig. 15.** Dependence of the strain energy $W^l$ (in units of $Db^3/[4(a+c)]$) of the rectangular prismatic dislocation loop on the normalized interspacing $d/b$ between its centre and the free surface, for $\nu = 0.3$, $r_0 = b$, $c/b = 10$ and $a/b = 5$, 10, 20, 40 and $\infty$ (curves 1, 2, 3, 4 and 5, respectively). Dashed lines correspond to values of $W^l_{max}$ and $W^l(\infty)$ for curve 3.

$$w_\perp^{dip(1)} = \lim_{c\to\infty}\frac{W^{l(1)}(d=c)}{2c}$$
$$\approx Db^2(1-\nu)\ln\frac{2a}{r_0}. \qquad (62)$$

The strain energy $W^{l(2)}$ of the second loop (Fig. 16b) reads [206]

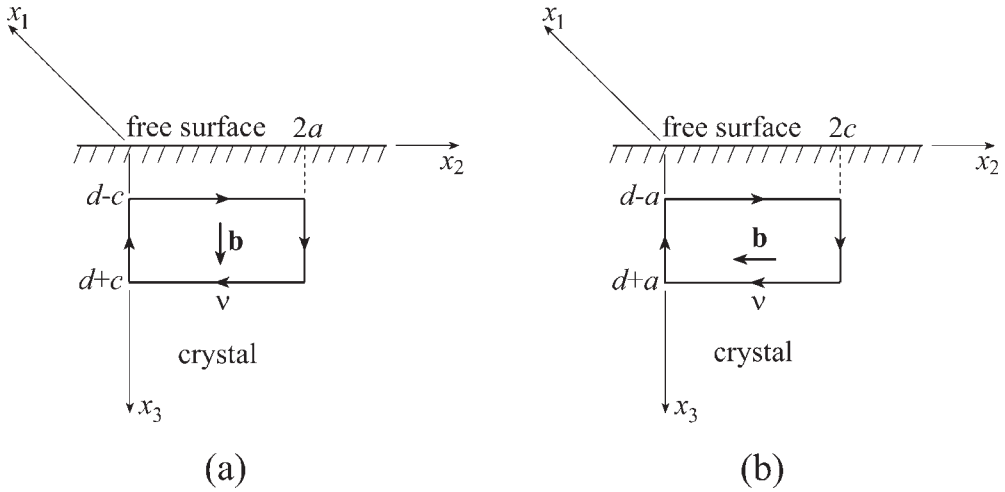


**Fig. 16.** Rectangular glide dislocation loops with the Burgers vectors (a) perpendicular and (b) parallel to the free surface of a half-space.

$$W^{l(2)} = \frac{Db^2}{4}\left\{(2-\nu)\ \bar{R}_1 + \frac{8\nu^2+3\nu-6}{3}\bar{R}_2 + 2(1-\nu)(1-2\nu)(x_3+x_3')\frac{x_3x_3'}{\bar{x}_2^2} + \left[\nu(3-2\nu)(x_3+x_3')^2 - 3x_3x_3'\right]\frac{2\bar{R}_2}{3\bar{x}_2^2} - (4\nu^2-2\nu-1)(x_3+x_3')\ln(x_3+x_3'+\bar{R}_2) - (x_3'-x_3)\ln(x_3'-x_3+\bar{R}_1) - (1-\nu)\bar{x}_2 \times \ln\frac{\bar{x}_2+\bar{R}_1}{\bar{x}_2+\bar{R}_2}\right\}\Bigg|_{x_2'=0}^{2c}\Bigg|_{x_3'=d-a}^{d+a}\Bigg|_{x_2=r_0}^{2c-r_0}\Bigg|_{x_3=d-a+r_0}^{d+a-r_0}. \quad (63)$$

In the limit as $d \to \infty$ formula (63) reduces to (19). For $c \to \infty$, the strain energy (63), divided by $2c$, transforms into the strain energy (per unit length) $w_{\parallel}^{dip(2)}$ of a dipole of screw dislocations that are parallel to the free surface. At $r_0 << a$, we obtain

$$w_{\parallel}^{dip(2)} = \lim_{c\to\infty}\frac{W^{l(2)}}{2c} = \frac{Db^2}{2}(1-\nu) \times\left[\ln\frac{d-a+r_0/2}{r_0/2} + \ln\frac{d+a}{r_0/2} - 2\ln\frac{d}{a}\right]. \quad (64)$$

For $d = a \to \infty$, the strain energy of the dislocation loop, divided by $2a$, is equal to the strain energy of a dipole of edge dislocations (per their unit length) whose lines are perpendicular to the free surface. At $r_0 << c$, this energy is determined by formula (60), where $a$ is replaced by $c$.

## 3.2. Disclinations near planar interfaces

As is the case with dislocations, we briefly discuss the most practical cases of straight disclinations and closed disclination loops.

### 3.2.1. Straight disclinations

The elastic behavior of straight disclinations parallel to flat interfaces in infinite or semi-infinite elastically isotropic medium was studied by Lejček [231], Zhukovskii [232], Romanov and Vladimirov [233-235], Romanov [236-238], and Yu and Sanday [239]. The principal solutions for elastic fields and energies are represented and discussed in detail in monographs of Vladimirov and Romanov [68,69], so that we do not consider them here but only give some remarks. The authors [231-234,236] examined the case of the free surface of a half-space. Vladimirov and Romanov [235] investigated disclination behavior near finite or infinite slipping boundaries in an elastically homogeneous infinite solid. Romanov [237,238] addressed the welded interphase boundaries, while Yu and Sanday [239] analyzed both the cases of welded and slipping interphase boundaries. Wedge disclinations were considered in [231-239], twist disclinations in [234,238,239]. It is worth noting that the solutions [232] and [239] are not convenient for checking and using in applications, because the first is given in the form of singular integrals, while the second is written in the most general form which needs multiple differentiation. In this sense, the solutions [231,233-238] are more preferable due to their compact analytical form.

The stress field and strain energy of a wedge disclination parallel to the free surface of an elastically anisotropic solid were found by Zembilgotov and Pertsev [240]. Wu [241] gave a detailed analysis of elastic stresses of a dipole of wedge disclinations placed near the interphase boundary in a transversally isotropic material. Recently he has extended this solution to the case of an infinite periodic row of wedge disclination dipoles which lie in the interphase boundary in such a material [242]. In his other recent work, Wu [243] has considered the strained state around a dipole of wedge interfacial disclinations in a hexagonal bicrystal with arbitrary in-plane $c$-axis orientations.

The disclinations emerging at flat free surfaces were examined by Romanov [244] and Belov [245]. By using a harmonic 3D stress function, Romanov [244] (see also [68,69,238]) obtained a simple closed analytical solution for the elastic stresses of a two-axes dipole of wedge disclinations perpendicular to the free surface of an elastically isotropic medium. Later this solution was derived as a limiting case of the solution of the more complicated problem for the same dipole in a thin plate [46,47]. Belov [245] considered a straight mixed disclination inclined under an arbitrary angle to the free surface of an elastically anisotropic half-space. In the special case of a wedge disclination in an elastically isotropic half-space, his general solution gives closed formulas for the field of displacements.

### 3.2.2. Disclination loops

For closed disclination loops, a few boundary-value problems were also solved. Circular twist disclination loops were examined by Chou [246,247], Chou and

Lu [248], Kuo and Mura [249], Kuo *et al.* [250] and Kolesnikova and Romanov [46,47], circular wedge disclination loops by Kuo and Mura [249], and Chou and Lu [251]. The disclination loops were placed near interphase boundaries [46,47,246,247,249,250] or free surfaces [248,251], and their planes were parallel to interfaces. Ding [252] found the stress fields for an infinitesimal disclination loop with arbitrary orientation of the Frank vector and for a similar finite-size rectangular loop, both lying in the interphase boundary. All the abovementioned solutions were obtained within the isotropic elasticity approach. A brief review of results [246-251] is given in [68,69]. An extended representation of the solutions [246-248,250] may also be found in [67].

Recently, the stress field of a circular twist disclination loop placed parallel to a free surface [46,47,247], has been used in solving the boundary-value problem for a nano- or micropipe (cylindrical cavity which contains a screw dislocation) having an axially symmetrical step at its surface and perpendicular to a flat free surface of a half-space [73].

## 3.3. Inclusions and inhomogeneities near planar interfaces

It seems that the first boundary-value problem for an inclusion was solved by Mindlin and Cheng [253]. They considered a spherical inclusion subjected to uniform dilatation eigenstrain and placed near the free surface of an elastically isotropic half-space. The eigenstrain was due to a difference in the coefficients of thermal expansion of the matrix and inclusion. The solution [253] is represented in the book by Melan and Parkus [82]. Recently, a similar solution has been obtained by Kolesnikova and Romanov [48] as a limiting case of the problem for the same inclusion in a thin plate. An extension of this solution to the case of an arbitrary uniform eigenstrain was done by Aderogba [254] who also found later a solution for the same inclusion near an interphase boundary [255].

The effect of flat free surfaces on the elastic fields of inclusions subjected to uniform eigenstrains was also studied by Chiu [256] for the case of a cuboidal inclusion and arbitrary eigenstrain, Seo and Mura [257] for an ellipsoidal inclusion with pure dilatation, Yu and Sanday [258] for an axisymmetric inclusion with pure dilatation or one-dimensional stretch eigenstrain. Interaction of a spheroidal inclusion with the free surface was considered by Loges *et al.* [259], who examined the interaction energy in dependence on the inclusion shape, size and orientation. Tsuchida *et al.* [107] and Jasiuk *et al.* [260] calculated the elastic fields of spherical inhomogeneities (i. e., incliusions which possess elastic moduli different from those of matrix) separated from matrix by welded or slipping boundaries and subjected to either uniform dilatation [107] or shear [260] eigenstrain, or external uniform one-dimensional [107] or shear [260] stress applied at the half-space surface. The physical impact of elastic interaction between a spherical inhomogeneity and a free surface was analyzed by Louat and Sadananda [261]. They demonstrated that the strained state around such an inhomogeneity (for example, an oxide particle in metallic matrix) may stimulate diffusion and result in formation of craters on the free surface. The elastic behavior of inclusions of different shapes near interphase boundaries was investigated by Korsunsky [262] and Walpole [263].

The main physical result, which follows from the aforementioned solutions, is that, as one could expect, any inclusion is attracted to a free surface due to the strain energy release. Most of these solutions are based on Eshelby's approach with taking into account the Green function of a half-space found by Mindlin [264]. It is worth noting that there was an error in sign in the original formulas of [264], which later was improved by the author. The corrected formulas are represented in the book by Mura [80] where the solution [257] is also given. The same method was used in calculations of thermal stresses created by a surface parallelepiped perturbed by a spherical inclusion [265] or a cylindrical inhomogeneous inclusion [266] in a half-space.

Yu and Sanday [267] suggested a different technique to consider the elastic behavior of a homogeneous isotropic inclusion of an arbitrary shape near flat interfaces. Based on Eshelby's approach, they noticed that the solution may be given in terms of the Galerkin vectors for nuclei of strain (e.g., unit concentrated force, double force, center of dilatation, etc., see the paper by Mindlin [268] for details) in a solid. In this case, instead of integration of elastic fields of a unit concentrated force over the inclusion volume (the Green function method), one has to integrate the linear superposition of the solutions for double force, double force with moment, and center of dilatation. Calculating first the solution for such a nucleus of strain in a bimaterial (two joined half-spaces with different elastic moduli) [269], the authors [267] then by simple integration obtained the solutions for the inclusion near both perfectly coherent and slipping interfaces. In the limiting cases,

when the elastic moduli of the neighbor phase were assumed to be equal to zero, and the inclusion shape was ellipsoidal or axisymmetric, the authors came to already known results for inclusions near a free surface [257,258].

The elastic anisotropy of a half-space was taken into account by Masumura and Chou [270] for the case of an elliptic inclusion subjected to antiplane eigenstrain. Zhang and Chou [271] extended this result to the interphase boundary between two half-spaces with different elastic anisotropies.

The elastic fields near inhomogeneities emerging at the flat free surface of a solid were calculated by Kouris and Mura [272] for hemispherical and Kouris et al. [273] for hemispheroidal inhomogeneities subjected to uniform eigenstrains or elastic strains caused by remote external loading. The same inhomogeneities were studied by Kouris [274] and Kouris and Tsuchida [275] with account for contact stresses. In all of these four cases, the authors considered and compared the solutions obtained for welded and slipping interfaces between the inhomogeneities and matrix. Kouris and Nuxoll [276] also solved a plane problem for inhomogeneity with hemicircular cross section in a half-space.

In the last decade, the interest to elastic behavior of inclusions and inhomogeneities of different shape near flat free surfaces and interphase boundaries has greatly grown due to appearance and development of nanotechnologies operating with quantum dotes and wires in semiconductor structures. A lot of new solutions has been obtained during this period. We can not consider them in the framework of the present review and address a reader to special reviews by Ovid'ko and Sheinerman [277], Maranganti and Sharma [151] and monograph by Ovid'ko and Sheinerman [278].

As an example, let us consider a long rod-like inclusion of rectangular cross section near a flat free surface (Fig. 17). The inclusion is subjected to pure dilatation eigenstrain $\varepsilon^*$ (see Section 2.3). In an infinite elastically isotropic solid, such an inclusion creates the stress field (35)-(36). For the case of a half-space, its stress field was derived in [58] through a limiting transition from the earlier solution obtained by Malyshev *et al.* [279] for the inclusion in a thin plate. In the coordinate system shown in Fig. 17, the solution [58] reads (in units of $2C$)

$$
\begin{aligned}
&\sigma_{11} = \sigma_{22} + \sigma_{33}, \quad \sigma_{12} = \sigma_{13} = 0,\\
&\sigma_{22} = \left[ \arctan\frac{a - x_2}{x_3' - x_3} + \arctan\frac{a + x_2}{x_3' - x_3} + 3\,\mathrm{arccotan}\frac{(x_3' + x_3)^2 + x_2^2 - a^2}{2a(x_3' + x_3)} \right.\\
&\qquad \left. - \frac{4ax_3\left[(x_3' + x_3)^2 - x_2^2 + a^2\right]}{\left[(x_3' + x_3)^2 + (a - x_2)^2\right]\left[(x_3' + x_3)^2 + (a + x_2)^2\right]} \right]\Bigg|_{x_3' = d - c}^{x_3' = d + c},\\
&\sigma_{33} = \left[ \arctan\frac{x_3' - x_3}{a - x_2} + \arctan\frac{x_3' - x_3}{a + x_2} + \mathrm{arccotan}\frac{(x_3' + x_3)^2 + x_2^2 - a^2}{2a(x_3' + x_3)} \right.\\
&\qquad \left. + \frac{4ax_3\left[(x_3' + x_3)^2 - x_2^2 + a^2\right]}{\left[(x_3' + x_3)^2 + (a - x_2)^2\right]\left[(x_3' + x_3)^2 + (a + x_2)^2\right]} \right]\Bigg|_{x_3' = d - c}^{x_3' = d + c},\\
&\sigma_{23} = \left[ \frac{1}{2}\ln\frac{\left[(x_3' - x_3)^2 + (a + x_2)^2\right]\left[(x_3' + x_3)^2 + (a - x_2)^2\right]}{\left[(x_3' - x_3)^2 + (a - x_2)^2\right]\left[(x_3' + x_3)^2 + (a + x_2)^2\right]} \right.\\
&\qquad \left. + \frac{8ax_2x_3(x_3' + x_3)}{\left[(x_3' + x_3)^2 + (a - x_2)^2\right]\left[(x_3' + x_3)^2 + (a + x_2)^2\right]} \right]\Bigg|_{x_3' = d - c}^{x_3' = d + c}.
\end{aligned}
\tag{65}
$$

The stress field (65) was used in modeling the physical mechanisms of plastic relaxation through generation of different configurations of misfit dislocations at the inclusion faces [58].

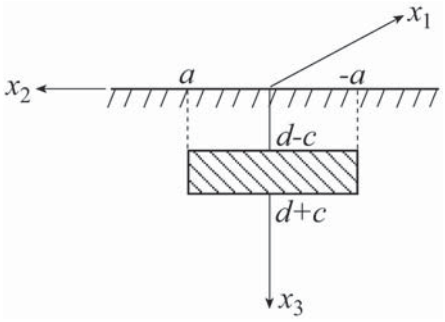


**Fig. 17.** A rod-like inclusion with rectangular cross section near the free surface of a half-space.

## 4. CONCLUSIONS

We have considered some basic solutions for the elastic fields and energies of dislocations, disclinations, inclusions and inhomogeneities located in infinite homogeneous media, near flat free surfaces of half-spaces, or in vicinity of interphase boundaries in infinite bi-materials. In parallel with results of traditional description of elastic behavior of defects within the classical linear theory of elasticity, we have also demonstrated some basic solutions obtained in the framework of the non-classical strain gradient theory of elasticity described by constitutive relation (4), and compared the results with those of nonlocal elasticity theory and gauge field theory of defects. It has been shown that the main achievement made in these non-classical approaches is the elimination of the classical singularities from the elastic fields at lines of dislocations and disclinations, as well as at edges of inclusions. A special attention has been paid to the stress fields and nanoscopic elastic behavior of dislocations near interfaces described in the framework of the strain gradient elasticity.

Summing up, there are many solutions obtained within the classical linear theory of elasticity, which may be used in theoretical description and modeling of defect structures in nanomaterials with several limitations. These limitations concern (1) strained state near dislocation and disclination lines, faces and edges of inclusions and inhomogeneities, where the classical elastic fields may diverge or suffer jump discontinuities; (2) short-range elastic interaction between the defects; and (3) short-range elastic interaction of defects with interfaces. The use of the strain gradient theory of elasticity allows one to dispense with these limitations. At the moment, there exist nonsingular gradient solutions for the fields of total displacements, elastic strains and stresses, and strain energies of straight dislocations in infinite homogeneous medium. There are nonsingular gradient solutions for elastic strains and stresses of straight disclinations, and elastic stresses of long rod-like inclusions with rectangular cross section in infinite homogeneous medium. There is a nonsingular gradient solution of the boundary-value problem for a straight dislocation near a welded interphase boundary. All these results may be applied to description of elastic behavior of defects in nanomaterials.

**ACKNOWLEDGEMENTS**

This work was supported by INTAS-AIRBUS program (grant 04-80-7339), Russian Fund of Basis Research (grant 04-01-00211), and Russian Science Support Foundation.

## REFERENCES

[1] M.Yu. Gutkin and I.A. Ovid'ko, *Plastic Deformation in Nanocrystalline Materials* (Springer, Berlin-Heidelberg-N.Y., 2004).

[2] A. Seeger, In: *Encyclopedia of Physics*, ed. by S. Flügge, Vol. VII, Part 1: Crystal Physics I (Springer, Berlin-Göttingen-Heidelberg, 1955).

[3] J. Friedel, *Dislocations* (Pergamon Press, Oxford-London-Edinburgh-N.Y.-Paris-Frankfurt, 1964).

[4] F.R.N. Nabarro, *Theory of Crystal Dislocations* (Oxford University Press, Oxford, 1967).

[5] J.P. Hirth and J. Lothe, *Theory of Dislocations*, 2nd edition (Wiley, N.Y. (NY), 1982).

[6] C. Teodosiu, *Elastic Models of Crystal Defects* (Springer, Berlin-Heidelberg-N.Y., 1982).

[7] D. Raabe, *Computational Materials Science: The Simulation of Materials, Microstructures and Properties* (Wiley-VCH, Weinheim-N.Y.-Chichester-Brisbane-Singapore-Toronto, 1998).

[8] A.E.H. Love, *A Treatise on the Mathematical Theory of Elasticity*, 4th edition (University Press, Cambridge, 1959).

[9] S.P. Timoshenko and J.N. Goodier, *Theory of Elasticity*, 3rd edition (McGraw Hill, Tokyo, 1970).

[10] R. de Wit // *J. Res. Nat. Bur. Stand.* (U.S.) **77A** (1973) 608.

[11] M.Yu. Gutkin // *Rev. Adv. Mater. Sci*. **1** (2000) 27.

[12] C. Malyshev // *Ann. Phys. (N.Y.)* **286** (2000) 249.
[13] M. Lazar // *Ann. Phys. (Leipzig)* **9** (2000) 461.
[14] M. Lazar // *Ann. Phys. (Leipzig)* **11** (2002) 635.
[15] M. Lazar // *J. Phys. A: Math. Gen.* **35** (2002) 1415.
[16] M. Lazar // *J. Phys. A: Math. Gen.* **35** (2002) 1983.
[17] M. Lazar // *Phys. Lett. A* **311** (2003) 416.
[18] M. Lazar // *J. Phys.: Condens. Matter* **15** (2003) 6781.
[19] M. Lazar // *Comput. Mater. Sci.* **28** (2003) 419.
[20] M. Lazar and G.A. Maugin // *Int. J. Eng. Sci.* **43** (2005) 1157.
[21] M. Lazar, G.A. Maugin and E.C. Aifantis // *Int. J. Solids Struct.* **43** (2006) 1787.
[22] M. Lazar and G.A. Maugin // *Proc. Roy. Soc. A* **462** (2006) 3465.
[23] C.Q. Ru and E.C. Aifantis, *Preprint* (MTU Report, Houghton, MI, 1993).
[24] M.Yu. Gutkin and E.C. Aifantis // *Scripta Mater.* **36** (1997) 129.
[25] M.Yu. Gutkin and E.C. Aifantis // *Phys. Stat. Sol.* (b) **214** (1999) 245.
[26] M.Yu. Gutkin and E.C. Aifantis // *Scripta Mater.* **40** (1999) 559.
[27] M.Yu. Gutkin and E.C. Aifantis, In: *Nanostructured Films and Coatings*, ed. by G.-M. Chow, I.A. Ovid'ko and T. Tsakalakos (Kluwer, Dordrecht, 2000).
[28] M.Yu. Gutkin and E.C. Aifantis // *Phys. Solid State* **41** (1999) 1980.
[29] M.Yu. Gutkin and E.C. Aifantis // *Scripta Mater.* **35** (1996) 1353.
[30] A.C. Eringen // *J. Phys. D: Appl. Phys*. **10** (1977) 671.
[31] A.C. Eringen // *J. Appl. Phys.* **54** (1983) 4703.
[32] A.C. Eringen, In: *The Mechanics of Dislocations*, ed. by E.C. Aifantis and J.P. Hirth (American Society for Metals, Metals Park, Ohio, 1985), p. 101.
[33] M.C. Valsakumar and D. Sahoo // *Bull. Mater. Sci*. **10** (1988) 3.
[34] D.G.B. Edelen // *Int. J. Eng. Sci.* **34** (1996) 81.
[35] M.Yu. Gutkin and E.C. Aifantis, Unpublished results (2003).
[36] E. Kröner. *Kontinuumstheorie der Versetzungen und Eigenspannungen* (Springer, Berlin-Göttingen-Heidelberg, 1958).
[37] F. Kroupa // *Czech. J. Phys. B* **10** (1960) 284; **12** (1962) 191.
[38] M.J. Marcinkowski and K.S. Sree Harsha // *J. Appl. Phys*. **39** (1968) 1775.
[39] M.J. Marcinkowski // *J. Appl. Phys*. **39** (1968) 4522.
[40] E.N. Mastrojannis, T. Mura and L.M. Keer // *Phil. Mag*. **35** (1977) 1137.
[41] N.J. Salamon and J. Dundurs // *J. Elast*. **1** (1971) 153.
[42] G. Eason, B. Noble and I.N. Sneddon // *Philos. Trans. R. Soc. London A* **247** (1955) 529.
[43] J. Dundurs and N.J. Salamon // *Phys. Stat. Sol*. (b) **50** (1972) 125.
[44] N.J. Salamon and M. Comninou // *Phil. Mag. A* **39** (1979) 685.
[45] N.J. Salamon and J. Dundurs // *J. Phys. C* **10** (1977) 497.
[46] A.L. Kolesnikova and A.E. Romanov, *Preprint of Ioffe Physico-Technical Institute*, No. 1019, Leningrad, 1986, in Russian.
[47] A.L. Kolesnikova and A.E. Romanov // *Phys. Solid State* **45** (2003) 1706.
[48] A.L. Kolesnikova and A.E. Romanov // *J. Appl. Mech*. **71** (2004) 409.
[49] V.I. Vladimirov, N.A. Pertsev and A.E. Romanov // *Mekh. Komp. Mater*. No.4 (1980) 730, in Russian.
[50] V.I. Vladimirov, N.A. Pertsev, N.D. Priemskii and A.E. Romanov // *Mekh. Komp. Mater*. No.3 (1982) 410, in Russian.
[51] V.I. Vladimirov, M.Yu. Gutkin, S.P. Nikanorov and A.E.Romanov // *Mekh. Komp. Mater*. No.4 (1986) 730, in Russian.
[52] K.L. Malyshev, M.Yu. Gutkin, A.E. Romanov, A.A. Sitnikova and L.M. Sorokin // *Sov. Phys.-Solid State* **30** (1988) 1176.
[53] M.Yu. Gutkin, I.A. Ovid'ko and Yu.I. Meshcheryakov // *J. Physique III (France)* **3** (1993) 1563.
[54] M.Yu. Gutkin, I.A. Ovid'ko and A.E. Romanov // *Radiat. Eff. Def. Solids* **129** (1994) 239.
[55] T.A. Khraishi and H.M. Zbib // *Phil. Mag. Lett*. **82** (2002) 265.
[56] Š. Verecký, J. Kratochvil and F. Kroupa // *Phys. Stat. Sol*. (a) **191** (2002) 418.
[57] M.Yu. Gutkin, *MS Thesis*, Leningrad Polytechnical Institute, 1985, in Russian.

[58] M.Yu. Gutkin, I.A. Ovid'ko and A.G. Sheinerman // *J. Phys.: Condens. Matter* **15** (2003) 3539.
[59] S.V. Bobylev, M.Yu. Gutkin and I.A. Ovid'ko // *Phys. Sol. State* **48** (2006) 1495.
[60] S.V. Bobylev, M.Yu. Gutkin and I.A. Ovid'ko // *Phys. Rev. B* **73** (2006) 064102.
[61] M.Yu. Gutkin and I.A. Ovid'ko // *Phil. Mag*. **86** (2006) 1483.
[62] M.Yu. Gutkin and I.A. Ovid'ko // *Appl. Phys. Lett*. **88** (2006) 211901.
[63] Yu.Z. Povstenko // *J. Phys. D: Appl. Phys*. **28** (1995) 105.
[64] R. de Wit, in: *Fundamental Aspects of Dislocations*, ed. by J.A. Simmons, R. de Wit and R. Bullough (Nat. Bur. Stand. (US), Spec. Publ. 317, vol. I, 1970), p. 651.
[65] R. de Wit // *J. Res. Nat. Bur. Stand. A* **77** (1973) 49, 359.
[66] R. de Wit, *Continual Theory of Disclinations* (Mir, Moscow, 1977), in Russian.
[67] V.A. Likhachev and R.Yu. Khairov, *Introduction to Disclination Theory* (Leningrad State University, Leningrad, 1975), in Russian.
[68] V.I. Vladimirov and A.E. Romanov, *Disclinations in Crystals* (Nauka, Leningrad, 1986), in Russian.
[69] A.E. Romanov and V.I. Vladimirov, in: *Dislocations in Solids*, ed. by F.R.N. Nabarro, v.9, (North Holland, Amsterdam, 1992), p. 402.
[70] Yu.Z. Povstenko // *Int. J. Engng. Sci.* **33** (1995) 575.
[71] M. Lazar and G.A. Maugin // *J. Mech. Phys. Solids* **52** (2004) 2285.
[72] A.G. Sheinerman and M.Yu. Gutkin // *Phys. Sol. State* **45** (2003) 1614.
[73] M.Yu. Gutkin and A.G. Sheinerman // *Phys. Stat. Sol*. (b) **241** (2004) 797.
[74] Yu.Z. Povstenko and O.A. Matkovskii // *Int. J. Solids Struct.* **37** (2000) 6419.
[75] N.A. Pertsev, A.E. Romanov and V.I. Vladimirov // *Phil. Mag. A* **49** (1984) 591.
[76] N.A. Pertsev, A.E. Romanov and V.I. Vladimirov // *J. Mater. Sci.* **16** (1981) 2084.
[77] N.A. Pertsev and A.E. Romanov // *Mekh. Komp. Mater.* No. 5 (1983) 781, in Russian.
[78] V.I. Vladimirov and N.A. Pertsev // *Mekh. Komp. Mater.* No. 4 (1984) 598, in Russian.
[79] N.A. Pertsev // *Mekh. Komp. Mater.* No. 1 (1987) 47, in Russian.
[80] T. Mura, *Micromechanics of Defects in Solids,* 2nd edition (Martinus Nijhoff Publishers, Dordrecht-Boston-Lancaster, 1987).
[81] J.N. Goodier // *Phil. Mag.* **23** (1937) 1017.
[82] E. Melan and H. Parkus, Wärmespannungen infolge stationärer Temperaturfelder (Springer, Wien, 1953).
[83] S.P. Timoshenko and J.N. Goodier, Theory of Elasticity (McGraw-Hill, New York, 1970).
[84] N.O. Miklestad // *J. Appl. Mech*. **9** (1942) A136.
[85] R.H. Edward // *J. Appl. Mech*. **18** (1951) 19.
[86] J.D. Eshelby // *Proc. Roy. Soc. London A* **241** (1957) 376.
[87] J.D. Eshelby // *Proc. Roy. Soc. London A* **252** (1959) 561.
[88] J.D. Eshelby, in: *Progress in Solid Mechanics*, Vol. 2, ed. by I.N. Sneddon and R. Hill (North-Holland, Amsterdam, 1961), p. 89.
[89] J.D. Eshelby. *Continual Theory of Dislocations* (Izdatelstvo inostrannoj literatury, Moscow, 1963), in Russian.
[90] I.A. Kunin and E.G. Sosnina // *Doklady AN SSSR* **199** (1971) 571, in Russian.
[91] M.A. Jaswon and R.D. Bhargava // *Proc. Camb. Phil. Soc*. **57** (1961) 669.
[92] J.R. Willis // *Quart. J. Mech. Appl. Math*. **17** (1964) 157.
[93] R.D. Bhargava and H.C. Radhakrishna // *J. Phys. Soc. Japan* **19** (1964) 396.
[94] L.J. Walpole // *Proc. Roy. Soc. London A* **300** (1967) 270.
[95] W.T. Chen // *Quart. J. Mech. Appl. Math*. **20** (1967) 307.
[96] R.D. List // *Proc. Camb. Phil. Soc*. **65** (1969) 823.
[97] R.J. Asaro and D.M. Barnett // *J. Mech. Phys. Solids* **23** (1975) 77.
[98] H.C. Yang and Y.T. Chou // *J. Appl. Mech*. **44** (1977) 437.
[99] A.A. Vakulenko and I.B. Sevostianov, in: *Studies on Mechanics of Building Constructions and Materials* (Izdatelstvo LISI, Leningrad, 1991) p. 8, in Russian.
[100] I.B. Sevostianov, in: *Fracture Mechanics. Theory and Experiment (Studies on Elasticity and Plasticity, Issue 17)* (St. Petersburg State University, St. Petersburg, 1995) p. 118, in Russian.
[101] I.B. Sevostianov, in: *Contiual Models of Discrete Systems*, Proc. 8th Intern. Symp., ed. by K.Z. Markov (Word Scientific Publ., Singapore, 1995) p. 573.
[102] T. Mura, H.M. Shodja and Y. Hirose // *Appl. Mech. Rev*. **49** (1996) S118.

[103] T. Mura and R. Furuhashi // *J. Appl. Mech.* **51** (1984) 308.
[104] T. Mura, I. Jasiuk and E. Tsuchida // *Int. J. Solids Struct*. **21** (1985) 1165.
[105] P.H. Leo, J. Iwan, D. Alexander and R.F. Sekerka // *Acta Metall*. **33** (1985) 985.
[106] T. Mura and M. Taya, in: *Recent Advances in Composites*, ed. by J.R. Vinsoin and M. Taya (ASTM, Philadelphia, 1985) p. 209.
[107] E. Tsuchida, T. Mura and J. Dundurs // *J. Appl. Mech.* **53** (1986) 103.
[108] J.H. Huang and T. Mura, in: *Defects and Anelasticity in the Characterization of Compatible Solids*, ed. by L.M. Brock (AMD, 1992, Vol. 148) p. 10.
[109] M. Lee, I. Jasiuk and E. Tsuchida // *J. Appl. Mech.* **59** (1992) S57.
[110] J.H. Huang and T. Mura, in: *Micromechanics of Random Media*, ed. by M. Ostoja-Starzewski and I. Jasiuk (Symp. Proc. ASCE-ASME-SES Joint Meeting, June 6-9, 1993) p. 10.
[111] S. Nemat-Nasser and M. Hori, *Micromechanics: Overall Properties of Heterogeneous Materials* (Elsevier Science Publishers B.V., Amsterdam-London-N.Y.-Tokyo, 1993).
[112] T. Mura // *Mater. Sci. Eng. A* **285** (2000) 224.
[113] N.A. Bert, A.L. Kolesnikova, A.E. Romanov and V.V. Chaldyshev // *Phys. Sol. State* **44** (2002) 2240.
[114] W. Nowacki, *Thermoelasticity* (Pergamon Press, New York, 1962).
[115] V.I. Lavrenyuk // *Izvestiya AN SSSR: Mekh. Tverd. Tela* No. 3 (1979) 63, in Russian.
[116] Ja.S. Podstrigatch, V.A. Lomakin and Yu.M. Kolyano, *Thermoelasticity of Heterogeneous Solids* (Nauka, Moscow, 1984), in Russian.
[117] S.L. Sass, T. Mura and J.B. Cohen // *Phil. Mag*. **16** (1967) 679.
[118] G. Faivre // *Phys. Stat. Sol*. **35** (1969) 249.
[119] R. Sankaran and C. Laird // *J. Mech. Phys. Solids* **24** (1976) 251.
[120] Y.P. Chiu // *J. Appl. Mech*. **44** (1977) 587.
[121] J.K. Lee and W.C. Johnson // *Phys. Stat. Sol*. (a) **46** (1978) 267.
[122] J.C.M. Li // *Metall. Trans. A* **9** (1978) 1353.
[123] A.G. Khachaturyan, *Theory of Structural Transformation in Solids* (Wiley, New York, 1983).
[124] L.M. Brown and D.R. Clarck // *Acta Metall*. **23** (1975) 821.
[125] G.C. Weatherly, P. Humble and D. Borland // *Acta Metall*. **27** (1979) 1815.
[126] K. Wakashima, K. Ishige and S. Umekawa // *Acta Metall*. **30** (1982) 1515.
[127] M. Hayakawa and M. Oka // *Acta Metall*. **9** (1984) 1415.
[128] M. Hong, D.E. Wedge and J.M. Morris // *Acta Metall*. **32** (1984) 279.
[129] R. Schneck, S.I. Rokhlin and M.P. Dariel // *Scripta Metall*. **18** (1984) 989.
[130] R. Monzen, K. Suzuki, A. Sato and T. Mori // *Acta Metall*. **31** (1983) 519.
[131] D.J. Srolovitz, R.A. Petkovic-Luton and M.J. Luton // *Phil. Mag. A* **48** (1983) 795.
[132] D.J. Srolovitz, M.J. Luton, R.A. Petkovic-Luton, D.M. Barnett and W.D. Nix // *Acta Metall.* **32** (1984) 1079.
[133] D.J. Srolovitz, R.A. Petkovic-Luton and M.J. Luton // *Scripta Metall.* **18** (1984) 1063.
[134] M. Taya and T. Mori // *Acta Metall*. **35** (1987) 155.
[135] K. Wakashima, B.H. Choi and T. Mori // *Mater. Sci. Eng. A* **127** (1990) 57.
[136] D.C. Dunand and A. Montensen // *Scripta Metall. Mater*. **25** (1991) 761.
[137] S. Shibata, M. Taya, T. Mori and T. Mura, in: *Proc. 12th Riso Intern. Symp. on Materials Science*, *1991*, p. 661.
[138] S. Shibata, T. Mori and M. Taya // *Scripta Metall. Mater*. **26** (1992) 363.
[139] M. Taya and T. Mori // *J. Eng. Mat. Tech*. **408** (1994) 408.
[140] M.Yu. Gutkin and A.E. Romanov // *J. Mech. Behav. Maters*. **6** (1996) 275.
[141] M.Yu. Gutkin, A.G. Sheinerman, T.S. Argunova, J.M. Yi, M.U. Kim, J.H. Je, S.S. Nagalyuk, E.N. Mokhov, G. Margaritondo and Y. Hwu // *J. Appl. Phys*. **100** (2006) 093518.
[142] M.Yu. Gutkin, I.A. Ovid'ko and N.V. Skiba // *Phys. Sol. State* **49** (2007) No.2.
[143] F. Kroupa and L. Lejček // *Czech. J. Phys. B* **20** (1970) 1063.
[144] M.Yu. Gutkin, V.R. Mirzoev, A.E. Romanov and M.E. Smagorinskii, in: *Physics of Strength of Heterogeneous Materials*, ed. by A.M. Leksovskii (Ioffe Physico-Technical Institute, Leningrad, 1988) p. 14.
[145] M.E. Smagorinskii, A.E. Romanov and M.Yu. Gutkin // *Russ. Metall. (USA)* No.3 (1990) 91.

[146] M.Yu. Gutkin, in: *XVI St. Petersburg Lecturing on Strength Problems*, 14-16 March 2006, Abstracts (St. Petersburg, 2006) p. 159, in Russian.
[147] B.S. Altan and E.C. Aifantis // *Scr. Metall. Mater.* **26** (1993) 319.
[148] N.M. Vlasov // *Phys. Sol. State* **43** (2001) 2083.
[149] A.C.E. Reid and R.J. Gooding // *Phys. Rev. B* **46** (1992) 6045.
[150] X. Zhang and P. Sharma // *Phys. Rev. B* **72** (2005) 195345.
[151] R. Maranganti and P. Sharma, in: *Handbook of Theoretical and Computational Nanotechnology*, ed. by M. Rieth and W. Schommers, Vol. 1 (American Scientific Publishers, 2006) p. 1.
[152] T. Mura, in: *Advances in Materials Research,* ed. by H. Herman, Vol. 3 (Interscience Publishers, New York-London-Sydney-Toronto, 1968) p. 1.
[153] J. Dundurs, in: *Mathematical Theory of Dislocations*, ed. by T. Mura (ASME, New York, 1969) p. 70.
[154] J.D. Eshelby, in: *Dislocations in Solids*, ed. by F.R.N. Nabarro, Vol. 1 (North-Holland, Amsterdam, 1979) p. 167.
[155] M.Yu. Gutkin and A.E. Romanov // *Phys. Stat. Sol.* (a) **125** (1991) 107.
[156] M.Yu. Gutkin, A.L. Kolesnikova and A.E. Romanov // *Mater. Sci. Eng. A* **164** (1993) 433.
[157] R. Bonnet // *Phys. Rev. B* **53** (1996) 10978.
[158] A.P. Sutton and R. Balluffi, *Interfaces in Crystalline Materials* (Clarendon Press, Oxford, 1995).
[159] A.E. Romanov, In: *Nanostructured Materials: Science and Technology*, ed. by G.-M. Chow and N.I. Noskova (Kluwer, Dordrecht, 1998) p. 207.
[160] M.Yu. Gutkin and I.A. Ovid'ko, *Physical Mechanics of Deformable Nanostructures*, Vol. 2: Nanolayered Structures (Yanus, St. Petersburg, 2005), in Russian.
[161] M.Yu. Gutkin, K.N. Mikaelyan and E.C. Aifantis // *Phys. Solid State* **42** (2000) 1652.
[162] M.Yu. Gutkin, K.N. Mikaelyan and E.C. Aifantis // *Scripta Mater.* **43** (2000) 477.
[163] K.N. Mikaelyan, M.Yu. Gutkin and E.C. Aifantis // *Phys. Solid State* **42** (2000) 1659.
[164] A.K. Head // *Phil. Mag*. **44** (1953) 92.
[165] A.K. Head // *Proc. Phys. Soc. London B* **66** (1953) 793.
[166] C.Q. Ru and E.C. Aifantis // *Acta Mechanica* **101** (1993) 59.
[167] L.A. Pastur, G.P. Feldman, A.M. Kosevich and V.M. Kosevich // *Fiz. Tverd. Tela* **4** (1962) 2585, in Russian.
[168] R. Siems, P. Delavignette and S. Amelinckx // *Phys. Stat. Sol*. **2** (1962) 636.
[169] Y.T. Chou // *Phys. Stat. Sol*. **15** (1966) 123.
[170] J. Gemperlová // *Czech. J. Phys. B* **18** (1968) 1085.
[171] J. Gemperlová // *Phys. Stat. Sol*. **30** (1968) 261.
[172] M.O. Tucker // *Phil. Mag.* **19** (1969) 1141.
[173] J. Braekhus and J. Lothe // *Phys. Stat. Sol*. (b) **43** (1971) 651.
[174] D.L. Clements // *Int. J. Engng. Sci*. **9** (1971) 257.
[175] C.S. Pande and Y.T. Chou // *J. Appl. Phys.* **42** (1971) 499.
[176] J.R. Willis // *J. Mech. Phys. Solids* **19** (1971) 353.
[177] C.S. Pande and Y.T. Chou // *J. Appl. Phys.* **43** (1972) 840.
[178] Y.T. Chou and C.S. Pande // *J. Appl. Phys.* **44** (1973) 3355, 5647.
[179] S. Nakahara and J.R. Willis // *J. Phys. F* **3** (1973) L249.
[180] D.M. Barnett and J. Lothe // *J. Phys. F* **4** (1974) 1618.
[181] Y.T. Chou and C.S. Pande // *J. Appl. Phys.* **45** (1974) 1447.
[182] Y.T. Chou, C.S. Pande and H.C. Yang // *J. Appl. Phys.* **46** (1975) 5.
[183] Y.T. Chou, C.S. Pande and H.C. Yang // *Mater. Sci. Engng.* **20** (1975) 19.
[184] M. Dupeux and R. Bonnet // *Acta Metall*. **28** (1980) 721.
[185] H.O.K. Kirchner // *Phil. Mag. A* **56** (1987) 583.
[186] C. Atkinson and D.A. Eftaxiopoulos // *Int. J. Fracture* **50** (1991) 159.
[187] T.C.T. Ting and D.M. Barnett // *Int. J. Solids Struct.* **30** (1993) 313.
[188] D.M. Barnett and J. Lothe // *Int. J. Solids Struct.* **32** (1995) 291.
[189] H.Y. Yu, S.C. Sanday, B.B. Rath and C.I. Chang // *Proc. Roy. Soc. London A* **449** (1995) 1.
[190] D.M. Barnett // *Scripta Mater.* **39** (1998) 371.
[191] D.M. Barnett, T.C.T. Ting and H.O.K. Kirchner // *Mater. Sci. Engng. A* **285** (2000) 18.

[192] H.Y. Yu and B.B. Rath // *Intern. Maters. Reviews* **45** (2000) 241.
[193] T.C.T. Ting and D.M. Barnett // *Math. Mech. Solids* **6** (2001) 3.
[194] H.Y. Yu // *J. Mech. Phys. Solids* **49** (2001) 261.
[195] M.S. Wu, H. Huang and R. Feng // *Mech. Maters.* **35** (2003) 913.
[196] B.T. Chen, C.T. Hu and S. Lee // *Int. J. Engng. Sci*. **36** (1998) 1011.
[197] E.H. Yoffe // *Phil. Mag.* **6** (1961) 1147.
[198] S.J. Shaibani and P.M. Hazzledine // *Phil. Mag. A* **44** (1981) 657.
[199] S.K. Maksimov, G.N. Gaidukov and A.P. Filippov // *Poverkhnost'* No.10 (1984) 95, in Russian.
[200] A.P. Filippov, G.N. Gaidukov and S.K. Maksimov // *Phys. Stat. Sol*. (a) **90** (1985) 215.
[201] A.Yu. Belov and V.A. Chamrov // *Metallofizika* **9**, No.3 (1987) 68, in Russian.
[202] V.L. Indenbom and G.N. Dubnova // *Fiz. Tverd. Tela* **9** (1967) 1171, in Russian.
[203] B. Honda // *Jap. J. Appl. Phys.* **18** (1979) 215.
[204] R. Arias and F. Lund // *J. Mech. Phys. Solids* **47** (1999) 817.
[205] A.G. Sheinerman and M.Yu. Gutkin // *Phys. Solid State* **45** (2003) 1694.
[206] M.Yu. Gutkin and A.G. Sheinerman // *Phys. Stat. Sol*. (b) **241** (2004) 1810.
[207] C.F. Hsieh and J. Dundurs // *Int. J. Engng. Sci*. **11** (1973) 933.
[208] J. Lothe // *Phys. Norvegica* **2** (1967) 153.
[209] J. Lothe, in: *Fundamental Aspects of Dislocation Theory*, ed. by J.A. Simmons, R. de Wit and R. Bullough, Vol. 1 (Nat. Bur. Stand. (US) Spec. Publ. No.317, New York, 1970) p. 11.
[210] J. Lothe, V.L. Indenbom and V.A. Chamrov // *Phys. Stat. Sol*. (b) **111** (1982) 671.
[211] A.Yu. Belov, V.A. Chamrov, V.L. Indenbom and J. Lothe // *Phys. Stat. Sol*. (b) **119** (1983) 565.
[212] A.Yu. Belov, in: *Elastic Strain Fields and Dislocation Mobility*, ed. by V.L. Indenbom and J. Lothe (Elsevier, 1992), p. 391.
[213] J.A. Steketee // *Canad. J. Phys.* **36** (1958) 192.
[214] L.V. Tikhonov // *Fiz. Metallov i Metalloved*. **24** (1967) 577 (in Russian).
[215] P.P. Groves and D.J. Bacon // *Phil. Mag.* **22** (1970) 83.
[216] D.J. Bacon and P.P. Groves, in: *Fundamental Aspects of Dislocation Theory*, ed. by J.A. Simmons, R. de Wit and R. Bullough, Vol. 1 (Nat. Bur. Stand. (US) Spec. Publ. No.317, New York, 1970) p. 35.
[217] I. Vagera // *Czech. J. Phys. B* **20** (1970) 702, 1278.
[218] R. Bonnet // *Phil. Mag. A* **47** (1983) 529.
[219] J. Baštecká // *Czech. J. Phys. B* **14** (1964) 430.
[220] S.D. Gavazza and D.M. Barnett // *Scripta Metall.* **9** (1975) 1263.
[221] W. Jäger, M. Rühle and M. Wilkens // *Phys. Stat. Sol*. (a) **31** (1975) 525.
[222] S.M. Ohr // *J. Appl. Phys.* **49** (1978) 4953.
[223] J. Dundurs and N.J. Salamon // *Phys. Stat. Sol*. (b) **50** (1972) 125.
[224] N.J. Salamon and J. Dundurs // *J. Phys. C* **10** (1977) 497.
[225] N.J. Salamon and M. Comninou // *Phil. Mag. A* **39** (1979) 685.
[226] N.J. Salamon // *J. Mech. Phys. Solids* **29** (1981) 1.
[227] H.Y. Yu and S.C. Sanday // *J. Phys.: Condens. Matter* **3** (1991) 3081.
[228] H. Koguchi // *JSME Intern. J. Ser. A – Sol. Mech. Mater. Eng*. **41** (1998) 465.
[229] J. Li and L. Li // *Prog. Nat. Sci*. **10** (2000) 183.
[230] L.M. Keer and I.A. Polonsky // *Phil. Mag. A* **67** (1993) 1423.
[231] L. Lejček // *Czech. J. Phys. B* **28** (1978) 434.
[232] I.M. Zhukovskii // *Fiz. Metallov i Metalloved*. **49** (1980) 7, in Russian.
[233] A.E. Romanov and V.I. Vladimirov // *Phys. Stat. Sol*. (a) **59** (1980) K159.
[234] A.E. Romanov and V.I. Vladimirov // *Phys. Stat. Sol*. (a) **63** (1981) 109.
[235] V.I. Vladimirov and A.E. Romanov // *Metallofizika* **4**, No.5 (1982) 12, in Russian.
[236] A.E. Romanov // *Phys. Stat. Sol*. (a) **63** (1981) 383.
[237] A.E. Romanov // *Poverkhnost'* No.12 (1985) 36, in Russian.
[238] A.E. Romanov, in: *Experimental Investigation and Theoretical Description of Disclinations*, ed. by V.I. Vladimirov (Ioffe Physico-Technical Institute, Leningrad, 1984), p. 110, in Russian.
[239] H.Y. Yu and S.C. Sanday // *Phys. Stat. Sol*. (a) **126** (1991) 355.

[240] A.G. Zembilgotov and N.A. Pertsev, in: *Disclinations and Rotational Deformation of Solids*, ed. by V.I. Vladimirov (Ioffe Physico-Technical Institute, Leningrad, 1988), p. 158, in Russian.
[241] M.S. Wu // *Int. J. Engng. Sci*. **38** (2000) 1811.
[242] M.S. Wu // *Int. J. Engng. Sci*. **40** (2002) 873.
[243] M.S. Wu // *Mathem*. *Mech. Sol*. **7** (2002) 541.
[244] A.E. Romanov // *Poverkhnost'* No.12 (1982) 121, in Russian.
[245] A.Yu. Belov. *Boundary-Value Problems in the Anisotropic Theory of Dislocations and Disclinations* (PhD Thesis, Shubnikov Institute of Crystallography, Moscow, 1987).
[246] T.-W. Chou // *J. Appl. Phys.* **42** (1971) 4092.
[247] T.-W. Chou // *J. Appl. Phys.* **42** (1971) 4931.
[248] T.-W. Chou and T.-L. Lu // *J. Appl. Phys.* **43** (1972) 2562.
[249] H.H. Kuo and T. Mura // *J. Appl. Phys.* **43** (1972) 3936.
[250] H.H. Kuo, T. Mura and J. Dundurs // *Int. J. Engng. Sci*. **11** (1973) 193.
[251] T.-W. Chou and T.-L. Lu // *Mater. Sci. Engng.* **12** (1973) 163.
[252] D.-H. Ding // *Phil. Mag. A* **56** (1987) 377.
[253] R.D. Mindlin and D.H. Cheng // *J. Appl. Phys.* **21** (1950) 931.
[254] K. Aderogba // *Math. Proc. Camb. Phil. Soc*. **80** (1976) 555.
[255] K. Aderogba // *Phil. Mag.* **35** (1977) 281.
[256] Y.P. Chiu // *J. Appl. Mech.* **45** (1978) 302.
[257] K. Seo and T. Mura // *J. Appl. Mech.* **46** (1979) 568.
[258] H.Y. Yu and S.C. Sanday // *J. Appl. Mech.* **57** (1990) 74.
[259] F. Loges, B. Michel and A. Christ // *Z. Angew. Math. Mech*. **65** (1985) 65.
[260] I. Jasiuk, P.Y. Sheng and E. Tsuchida // *J. Appl. Mech.* **64** (1997) 471.
[261] N. Louat and K. Sadananda // *Phil. Mag. A* **64** (1991) 213.
[262] A.M. Korsunsky // *J. Appl. Mech.* **64** (1997) 697.
[263] L.J. Walpole // *IMA J. Appl. Math.* **59** (1997) 193.
[264] R.D. Mindlin, in: *Proc. 1st Midwestern Conf. on Solid Mech.* (University of Illinois, Urbana, IL, 1953) p. 55.
[265] S. Lee and C.C. Hsu // *Acta Metall*. **33** (1985) 985.
[266] H. Hasegawa, R.H. Liang and T. Mura // *J. Thermal Stresses* **15** (1992) 295.
[267] H.Y. Yu and S.C. Sanday // *Proc. Roy. Soc. London A* **434** (1991) 521.
[268] R.D. Mindlin // *Physics* **7** (1936) 195.
[269] H.Y. Yu and S.C. Sanday // *Proc. Roy. Soc. London A* **434** (1991) 503.
[270] R.A. Masumura and Y.T. Chou // *J. Appl. Mech.* **49** (1982) 52.
[271] H.T. Zhang and Y.T. Chou // *J. Appl. Mech.* **52** (1985) 87.
[272] D.A. Kouris and T. Mura // *J. Mech. Phys. Solids* **37** (1989) 365.
[273] D.A. Kouris, E. Tsuchida and T. Mura // *J. Appl. Mech.* **56** (1989) 70.
[274] D.A. Kouris // *European J. Mech., A/Solids* **9** (1990) 551.
[275] D.A. Kouris and E. Tsuchida // *European J. Mech., A/Solids* **11** (1992) 323.
[276] D.A. Kouris and J.P. Nuxoll // *Acta Mech*. **97** (1993) 169.
[277] I.A. Ovid'ko and A.G. Sheinerman // *Rev. Adv. Mater. Sci*. **9** (2005) 17.
[278] I.A. Ovid'ko and A.G. Sheinerman. *Nanomechanics of Quantum Dots and Wires* (Yanus, St. Petersburg, 2004), in Russian.
[279] K.L. Malyshev, M.Yu. Gutkin, A.E. Romanov, A.A. Sitnikova and L.M. Sorokin, *Preprint of Ioffe Physico-Technical Institute*, No. 1109, Leningrad, 1987, in Russian.